

1 Responses of estuarine circulation to the morphological evolution in a
2 convergent, microtidal estuary

3 Rui Zhang^a, Bo Hong^b, Lei Zhu^{a,c,d}, Wenping Gong^{a,c*}, Heng Zhang^{a,c,d}

4 a- School of Marine Sciences, SunYat-sen University, Guangzhou, China, 510275

5 b- School of Civil and Transportation Engineering, South China University of
6 Technology, Wushan RD., Tianhe District, Guangzhou 510641, China

7 c- Southern Marine Science and Engineering Guangdong Laboratory (Zhuhai), Zhuhai
8 519000, China

9 d- Pearl River Estuary Marine Ecosystem Research Station, Ministry of Education,
10 Zhuhai, 519082, China

11
12 **Abstract:**

13 The Huangmaohai Estuary (HE) is a funnel-shaped microtidal estuary in the west
14 of the Pearl River Delta (PRD) in southern China. Since China's reform and opening up
15 in 1978, extensive human activities have occurred and greatly changed the estuary's
16 topography, and modified its hydrodynamics. In this study, we examined the
17 morphological evolution by analyzing remote sensing data with ArcGIS tools and
18 studied the responses of hydrodynamics to the changes in topography from 1977 to
19 2010 by using the Delft3d model. We took the changes in estuarine circulation during
20 neap tides in dry seasons as an example. The results show that human reclamation
21 caused a narrowing of the estuary, and channel dredging deepened the estuary. These
22 human activities changed both the longitudinal and lateral estuarine circulations. The
23 longitudinal circulation was observed to increase with the deepening and narrowing of
24 the estuary. The lateral circulation experienced changes in both the magnitude and
25 pattern. The momentum balance analysis shows that when the depth and width changed
26 simultaneously, the longitudinal estuarine circulation was modulated by both the

* Supported by the National Natural Science Foundation of China under contract Nos 51761135021,
41506102 and 41890851.

** Corresponding author, E-mail: gongwp@mail.sysu.edu.cn

27 channel deepening and width reduction, in which the friction, pressure gradient force,
28 and advection terms were altered. The analysis of the longitudinal vortex dynamics
29 indicates that the changes in the vertical shear of the longitudinal flow, lateral salinity
30 gradient, and vertical mixing were responsible for the change in the lateral circulation.
31 The changes in water depth are the dominant factor affecting lateral circulation intensity.
32 This study has implications for sediment transport and morphological evolution in
33 estuaries heavily impacted by human interventions.

34

35 **Keywords:** Estuarine circulation, Morphological evolution, Huangmaohai Estuary

36

37 **1. Introduction**

38

39 Estuarine circulation, the tidally averaged flow in estuaries including both the
40 longitudinal and lateral circulations, is the main driving force for the transport of
41 sediment, pollutants, and other materials, and also one of the primary factors affecting
42 the ecological environment of estuaries (Kjerfve et al., 1981). Estuarine circulation is
43 influenced by many factors (Geyer and Maccready, 2014), such as sea-level
44 fluctuations (Wilson and Filadelfo, 1986), river discharge, tides (Pritchard, 1952), and
45 winds (Scully et al., 2005; Waterhouse et al., 2013; Geyer and Maccready, 2014; Salles
46 et al., 2015; Chen et al., 2020a). Topography in an estuary has a significant effect on
47 the pattern and intensity of the estuarine circulation (Fischer, 1976; Dyer, 1977).
48 Human activities may change the estuarine topography, leading to changes in the
49 estuarine circulation and associated material transport. Therefore, a study of the
50 estuarine circulation and its response to human activities is essential for integrated
51 management of the development of estuarine resources, and the maintenance of the
52 estuary's ecological health.

53 Channel deepening by dredging and sand mining is a common practice in the
54 development and maintenance of navigable channels ~~and resource utilization~~ in
55 estuaries. Generally speaking, channel deepening can increase the longitudinal

56 estuarine circulation by decreasing the bottom friction and increasing the baroclinic
57 forcing which is proportional to the water depth (Amin, 1983; Chernetsky et al., 2010;
58 Winterwerp, 2011). On the other hand, the increase in water depth can also increase the
59 salt intrusion and decrease the horizontal density gradient, thus reducing the baroclinic
60 force. Channel deepening also affects the estuarine circulation in other ways, such as
61 increasing the Stokes transport and the associated compensating return flow (Amin,
62 1983), altering the nonlinear tidal rectification (Li and O'Donnell, 1997), and tidal
63 asymmetry in mixing between flood and ebb tides (tidal straining) (Simpson, 1990).
64 Therefore, the effect of channel deepening is an intricate balance between these
65 reinforcing and/or competing effects. Chant et al. (2018) demonstrated that a relatively
66 small (15%) increase in water depth can result in a double exchange flow. They
67 attributed this increase to the increase in horizontal salinity gradient and/or a reduction
68 in vertical mixing, but they did not give a clear distinction about how these two effects
69 work together and which is dominant.

70 Change in estuary width is another aspect of topographic change in estuaries and
71 is mainly caused by reclamation and utilization of salt marshes, construction of coastal
72 protection structures along the estuarine banks. Change in estuary width generates a
73 change in the estuarine convergence, and therefore a change in the estuarine circulation.
74 Burchard et al. (2014) concluded that an increase in the estuarine convergence results
75 in an enhancement or reduction of the longitudinal estuarine circulation as increased
76 estuarine convergence can reduce or even reverse the straining-induced circulation,
77 though the advection-induced circulation is increased. Changes in estuarine width can
78 also modify the lateral circulation and feedback to the generation of the longitudinal
79 estuarine circulation through the change in lateral advection (Lacy et al., 2003; Lerczak
80 and Rockwell Geyer, 2004; Scully et al., 2009; Burchard et al., 2010; Burchard et al.,
81 2014). Lerczak and Rockwell Geyer (2004) suggested that lateral effects on the
82 longitudinal estuarine circulation would be stronger in narrower estuaries given a
83 constant lateral salinity gradient. Schulz et al. (2015) investigated the impact of the
84 depth-to-width ratio of the estuarine cross-section on the longitudinal estuarine

85 circulation and found that the longitudinal estuarine circulation exhibits a distinct
86 maximum in medium-wide channels. They diagnosed the mechanisms for such a
87 phenomenon and attributed it to the sensitivities of the straining- and advection-induced
88 circulations on the changes in depth-to-width ratio.

89 As revealed by Lerczak and Geyer (2004) and other researchers (Chen et al.,
90 2020b), lateral processes play important roles in the generation of the longitudinal
91 estuarine circulation. ~~The lateral circulation can modify the longitudinal estuarine~~
92 ~~circulation by the lateral redistribution of the longitudinal current in a direct way~~
93 ~~(Lerczak and Geyer, 2004), and change the longitudinal pressure gradient force and the~~
94 ~~friction in an indirect way.~~ In estuaries, the pattern and intensity of lateral circulation
95 are controlled by three processes (Li et al., 2014): vertical shear of the longitudinal
96 current affecting the tilting of planetary vorticity, lateral salinity gradient (baroclinicity),
97 and diffusion. The longitudinal estuarine circulation can affect the lateral circulation
98 through all the mentioned three factors. Therefore, the interaction between the
99 longitudinal and lateral processes is fully nonlinear and quite complex. Though these
100 interactions have been discussed in detail (Scully et al., 2009; Li et al., 2017), several
101 questions remain open: How does the longitudinal estuarine circulation affect the
102 intensity and vortex structure of the lateral circulation? Does a decreased/increased
103 lateral circulation necessarily lead to a weakened/strengthened longitudinal circulation?
104 These questions become complicated in an estuary where both width and depth vary.
105 Previous studies showed that the narrowing and deepening of the Yangtze River
106 Estuary resulted in an enhanced longitudinal estuarine circulation (Zhu, 2018), which
107 changed from transversely sheared to vertically sheared. The estuarine stratification
108 was also found to be strengthened, along with an increase in the intensity of lateral
109 circulation. Zhu et al. (2015) investigated the influences of channel deepening and
110 widening on the tidal and nontidal circulations of Tampa Bay, USA, and found that the
111 nontidal circulation was strengthened by these human interventions. However, how
112 does the estuarine circulation respond to both narrowing and deepening/shallowing of
113 the estuary? What happens when the narrowing rate is much larger or smaller than the

114 deepening rate in an estuary? Here the narrowing rate is the ratio of the difference of
115 cross-section widths between two consecutive years divided by the width in the earlier
116 year. Similarly, the deepening rate is the ratio of the difference of water depth in the
117 cross-section between the two consecutive years divided by the earlier year's depth.

118 Here we try to address the above questions by studying the changes in the estuarine
119 circulation ~~via using the historical topographic data obtained~~ from 1977 to 2010 in the
120 Huangmaohai Estuary (HE). ~~The HE is,~~ a microtidal estuary in the southwest of the
121 Pearl River Delta (PRD), ~~and which~~ experienced different stages of topographic
122 changes under human activities ~~from 1977 to 2010, which can be grouped into two~~
123 ~~scenarios:~~ narrowing and deepening (1977-1994, and 2003-2010), and narrowing and
124 shallowing (1994-2003). ~~These two scenarios of topographic changes caused different~~
125 ~~responses of the estuarine circulation, and t~~ Thus, it provided a good opportunity to
126 study the effect of human activities induced morphological evolution on the estuarine
127 circulation.

128 In this study, we used a state-of-the-art three-dimensional baroclinic model (Delft
129 3d) to simulate the changes in hydrodynamics in the HE in different years and examined
130 the changes in intensities of the longitudinal and lateral estuarine circulations, followed
131 by an analysis of the mechanisms for these changes by conducting diagnostic analyses
132 of the momentum balance. The structure of the rest of the paper is as follows. Section
133 2 introduces the study area and numeral model ~~(including model setting and validation).~~
134 Section 3 presents the results of morphological evolution and changes in the estuarine
135 circulation. Then, the mechanisms for the changes in estuarine circulation are
136 investigated using the momentum and vortex balance equations in Section 4. Finally,
137 the conclusions are presented in Section 5. ~~For the sake of conciseness, we append a~~
138 ~~supplement in the appendix about the model validation for water level, current, and~~
139 ~~salinity.~~

140

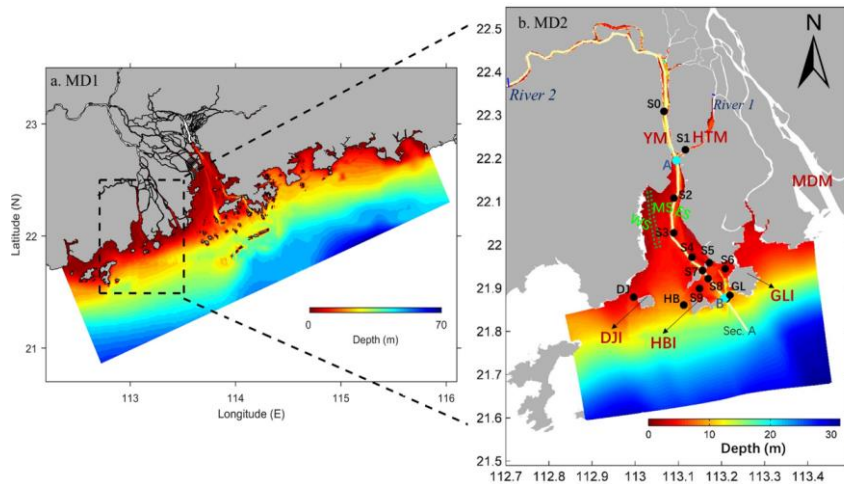
141 2. Study area and methodology

142

143 **2.1 Study area**

144

145 The HE is located in the west of the PRD in southern China and exhibits a
146 distinctly convergent geometry, with a latitude ranging from 21 °50' to 22 °13' N and
147 a longitude ranging from 113 °00' to 113 °51' E (Fig. 1). The estuary is composed of a
148 bay (Huangmao Bay) and a tidal river. The bay is trumpet-shaped with an area of 409
149 km². It has a complex bathymetry comprising of two channels and three shoals, namely
150 the West Channel and East Channel, the West Shoal, Middle Shoal, and East Shoal. In
151 recent decades, the West Channel is observed to shrink and almost disappear now (Jia
152 et al., 2012). The width of the bay is 30 km at the estuary mouth and decreases to 1.8
153 km at the head. The mean water depth of the bay is 4.5 m (Gong et al., 2014). The bay
154 is connected to the upstream river catchment by two constrictions (Yamen and
155 Hutiaomen Outlets). Several islands, namely Dajin Island, Hebao Island, and Gaolan
156 Island, are scattered at the estuary's mouth. ~~The estuary mouth is divided into three~~
157 ~~entrances: the West Entrance between the Dajin Island and the western shore; the~~
158 ~~Central Entrance between the Dajin Island and the Hebao Island, where the West~~
159 ~~Channel passes through; and the East Entrance between the Hebao Island and the~~
160 ~~Gaolan Island, where the East Channel goes through~~ (shown in Fig. 1b).



161

162

163 Fig. 1. The study area (Huangmaohai estuary) and observation stations. Major topographic
 164 features and domains of the nested modeling system over (a) the PRD and (b) the HE and its
 165 adjacent waters. YM = Yamen; HTM = Hutiaomen; MDM = Modaomen; DJI = Dajing Island;
 166 GLI = Gaolan Island; HBI = Hebao Island. The black dots (S0–S9, DJ, HB, and GL) in the
 167 MD2 domain are stations of field deployments in March 2010. The solid lines represent the
 168 along-channel transect (Section A (AB)), which lies in the East Channel. The green dotted lines
 169 represent the West Channel in 1977. Three shoals are shown in (b): West Shoal (WS), Middle
 170 Shoal (MS), and East Shoal (ES).

171

172 The HE has a subtropical monsoon climate, with the precipitation in the wet season
 173 (from May to September) being high. Approximately 80% of the river discharge occurs
 174 during the wet season, with an average discharge of 200.23 m³/s. The tides in the HE
 175 are mixed semidiurnal with dominant semi-diurnal constituents and smaller diurnal
 176 constituents. ~~The tides show obvious asymmetry in terms of tidal duration, velocity,
 177 and current acceleration between floods and ebbs (Gong et al., 2016).~~ The tidal range
 178 is approximately 1.5 m at the mouth and experiences an initial increase from the mouth
 179 towards the head owing to a strong convergence of the bay width. Further landward in
 180 the tidal river beyond the bay head, the tidal range decreases by the overwhelming
 181 bottom friction (Gong et al., 2012). The tidal current velocity ranges from 0.5 m/s to
 182 1.5 m/s (Huang, 2011), and is higher in deep channels than on shallow shoals. The tidal

183 currents are generally rectilinear in deep channels but become more rotary in shallow
184 shoals.

185 Since the 1980s, human activities have been intense in the HE-estuary. A
186 hydroelectric power project upstream of the estuary, channel dredging, sand mining,
187 and construction of Gaolan Island levees have led to great changes in the HE's
188 topography. Also, the HE has rich tidal flat resources and endured frequent reclamation
189 activities. From 1965 to 2003, a total of 142.29 km² tidal flat was reclaimed, with an
190 average reclamation rate of 3.74 km²/a, and the reclamation rate continuously but
191 gradually increased during that period. After 2003, the reclamation rate slowed down.
192 In terms of channel dredging, the Yamen Waterway Project was conducted in 1997 to
193 deepen the channel between S0 and S3 in Fig. 1b (Luo, 2010). In April 2005, the Yamen
194 Channel regulation project was implemented to alleviate the serious siltation in the
195 channel, with the channel being dredged to a depth of about 6 m.

196 In the following, we chose 1977, 1994, 2003, and 2010 as the representative years
197 to study the typical scenarios of bathymetric changes in the HE.

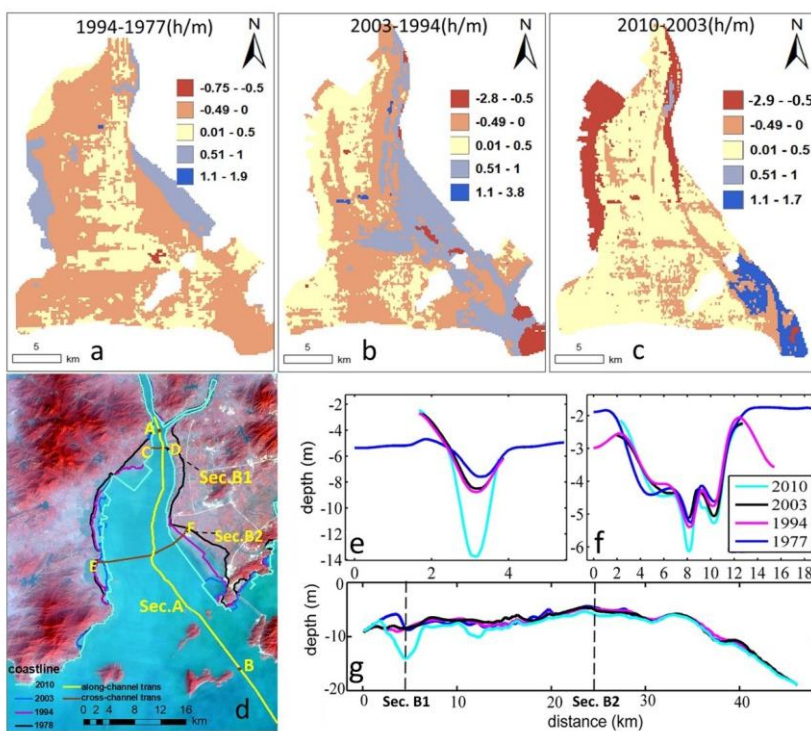
198

199 **2.2 Remote sensing and topographic data**

200

201 Remote sensing data were used for coastline extraction and included Landsat
202 Multi-Spectral Scanner (MSS) data, Landsat Thematic Mapper (TM) data, and Landsat
203 Operational Land Imager (OLI) data. A total of ~~142G data of~~ 66 images (Table 1)
204 ~~covering the PRD during cloudless days in multiple years (from 1973 to 2018)~~ were
205 downloaded from <http://www.gscloud.cn/>. These data were firstly processed by
206 geometric ~~(with the errors were shown to be less than 0.5 pixels (Ai et al., 2019))~~ and
207 atmospheric corrections by the ENVI 5.3 software. ~~Subsequently, they were compared~~
208 ~~with topographic data for further geometric corrections. The errors were shown to be~~
209 ~~less than 0.5 pixels (Ai et al., 2019).~~ The topography data inside the HE were derived
210 from nautical charts (1977, 1994, 2003, and 2010), published by the Navigation Safety
211 Guarantee Bureau. The filling and excavation toolbox of ArcGIS was used to calculate

212 the difference between the volumes in two consecutive periods by superimposing the
 213 corresponding Digital Elevation Models (DEM). ~~This method is actually to decompose~~
 214 ~~three dimensional space entities into many cuboids, then calculate the differences of~~
 215 ~~area and volume of each cuboid between two consecutive years, and classify the~~
 216 ~~cuboids into different categories based on the siltation thickness.~~ We thus obtained the
 217 average siltation rates of the study area over different years (Figs. 2a-c).



218 Fig. 2. (a-c) Water depth difference between two consecutive years ((a)1994-1977; (b)2003-
 219 1994; (c)2010-2003), where the positive value indicates “deepening” and the negative one
 220 indicates “siltation”, (d) Shorelines of 1977-2010 and locations of two cross-sections (AB: Sec.
 221 A; CD: Sec. B1; EF: Sec. B2); (e, f, and g) The bathymetric evolutions at Sections B1, B2, and
 222 A in 1977, 1994, 2003, and 2010.
 223
 224
 225
 226
 227

Table 1. Data of remote sensing images

Time	Satellite	Image sensor	Resolution/m	Path/Row	Memory space
1973,1978	Landsat3	MSS	78		
1986-2011	Landsat5	TM	30	122/45	142G
2012	Landsat7	ETM	30		
2013-2018	Landsat8	OLR	30		

228
229
230

231 2.3 Numerical model setting up and validation

232

233 The numerical model Delft3d, a fully three-dimensional hydrodynamic water
234 quality model (Lesser et al., 2004), was used to simulate the hydrodynamics in the HE.
235 ~~The Delft3d model is a fully three-dimensional hydrodynamic water quality model, and~~
236 ~~can accurately simulate large-scale flow, water quality, and morphological evolution~~
237 ~~(Lesser et al., 2004). The Its algorithm of the Delft3d model can guarantee the~~
238 conservation of mass, momentum, and energy. The model grid consisted of a nesting
239 grid system, with the MD1 (parent model, Fig. 1a) covering the whole PRD, and the
240 MD2 (child model) covering the HE. For the MD2 model, a curvilinear orthogonal grid
241 ~~an orthogonal Cartesian horizontal grid~~ of 269*620 was established, with the horizontal
242 resolution ranging from 85 m in the channel to 324 m at the ocean boundary. Vertically,
243 the grid was discretized into 10 layers of σ coordinate. The model system used here is
244 the same as the one in Chen et al. (2020a). Briefly, the open boundary conditions of the
245 MD1 model included atmospheric forcing at the water surface, river discharge at the
246 upstream boundary, tidal and non-tidal water elevations and currents, a constant salinity
247 of 34 psu at the open ocean boundary. The results from the MD1 were interpolated to
248 provide ocean boundary conditions for the MD2 model.

249 As mentioned above, the hydrodynamics in the HE experiences distinct seasonal
250 variation. The estuarine circulation during the wet season has been extensively studied
251 before (Chen et al., 2020a; Chen et al., 2020b). Here we choose the dry season to
252 investigate the changes in the estuarine circulation caused by topographic changes in

253 different years. We conducted a series of numerical experiments using the bathymetry
 254 data in 1977, 1994, 2003, and 2010. The simulation time was chosen to be from 00:00
 255 on March 1 to 23:00 on March 31 in the dry season, when observation data were
 256 available in 2010. Field measurements were carried out at 14 mooring stations on
 257 March 17th 17:00 to 18th 22:00, 2010. ~~The measured variables included vertical~~
 258 ~~profiles of current, temperature, and salinity. In these surveys, ADCP was utilized to~~
 259 ~~measure the vertical profile of current with a vertical resolution of 0.3 m and a time~~
 260 ~~resolution of 5 min, and CTD was used to measure the vertical profiles of salinity and~~
 261 ~~temperature every hour. Hourly data were obtained after post-processing of the raw~~
 262 ~~data and used for model validation here.~~ In all the four scenarios, two upstream
 263 boundaries were specified (Fig. 1b): at River 2 by specifying real-time water level data
 264 from the MD1 model from 00:00 on March 1, 2010, to 23:00 on March 31, 2010, with
 265 a time interval of 1 hour; At River 1 by specifying a constant river discharge of $100 \text{ m}^3 \text{ s}^{-1}$
 266 ~~2~~. The choice of this constant value was based on ~~the~~ previous simulation experiences
 267 (Chen et al., 2020a; Chen et al., 2020b). The salinities at the river inflow boundaries
 268 were set to be 0 psu. The only changing condition of the four scenarios was the
 269 topography (Table 2), so the effect of topographic change can be ~~identified~~
 270 ~~distinguished~~. The measured data from 14 stations in 2010 were used to validate the
 271 model. ~~The validation included water level, current direction and magnitude, and~~
 272 ~~salinity (Figs. A. 1-4).~~

273

274 Table 2. Coastline, bathymetries, salinity, flow, and tidal boundary in the four model scenarios.

Scenario	Coastline	Bathymetrie s	The salinity of the open sea	Flow	Tidal boundary
1977/03	1977	1977	2010/03	2010/03	2010/03
1994/03	1994	1994	2010/03	2010/03	2010/03
2003/03	2003	2003	2010/03	2010/03	2010/03
2010/03	2010	2010	2010/03	2010/03	2010/03

275

276 In this study, the Willmott skill score (SK) was used to evaluate whether the model
 277 result is consistent with the observed data (Willmott, 1981). The SK is defined as:

$$SK = 1 - \frac{\sum_{i=1}^n (O_i - M_i)^2}{\sum_{i=1}^n (|M_i - \bar{O}| + |O_i - \bar{O}|)^2}, \quad (1)$$

where n is the number of the observed data, M and O are model simulation results and observations, respectively, and \bar{O} is the average value of the observation data. SK is used to measure the consistency between the model results and the observations, with a value between 0 and 1. The larger the value is, the more consistent the simulation results are with the observed data.

Firstly, the water level of the MD2 model was validated (Fig. A. 1). The SKs of the four observed stations are all above 0.86, indicating that the water level simulation is reasonable. Secondly, the modeled current directions showed good performance except for the surface layer at Stations DJ and S0 (Fig. A. 2), almost all the SKs are greater than 0.7 (Table 3). The simulation of current speed (Fig. A. 3) is worse than that of the current direction, but the SKs at most stations are above 0.6, showing a good performance. ~~We note that the SK (less than 0.4) at Station S3 is significantly lower than other stations, mostly because the station was located near the null point (the convergence point between seaward and landward bottom residual flows) and the current speed was quite small.~~ Lastly, the trends of observed and simulated salinities are consistent (Fig. A. 4), and almost all the SKs of salinity validation are above 0.5, especially in S1-S3, showing a good performance of the salinity simulation.

Table 3. Skill scores by comparison of modeled results with observations.

Stations	Current direction			Current speed			Salinity		
	Sur	Mid	Bot	Sur	Mid	Bot	Sur	Mid	Bot
S0	0.18	0.96	0.96	0.77	0.88	0.86	0.32	0.35	0.35
S1	0.94	0.99	0.99	0.65	0.66	0.61	0.94	0.94	0.90
S2	0.78	0.79	0.71	0.83	0.84	0.84	0.84	0.85	0.85
S3	0.87	0.98	0.95	0.34	0.38	0.39	0.92	0.79	0.77
S4	0.84	0.94	0.94	0.53	0.55	0.53	0.77	0.64	0.54
S5	0.86	0.92	0.93	0.66	0.71	0.72	0.37	0.25	0.26
S6	0.79	0.90	0.88	0.68	0.75	0.74	0.15	0.20	0.25
S7	0.82	0.85	0.96	0.74	0.79	0.83	0.86	0.66	0.56
S8	0.84	0.89	0.89	0.59	0.62	0.66	0.82	0.77	0.72
S9	0.80	0.74	0.77	0.54	0.46	0.41	0.59	0.50	0.52
DJ	0.61	0.77	0.77	0.38	0.47	0.51	0.66	0.47	0.37

GL	0.89	0.91	0.93	0.50	0.51	0.49	0.37	0.43	0.41
HB	0.71	0.89	0.89	0.60	0.56	0.56	0.57	0.54	0.53

298

299

300

301

302

303

304

305

306

307

308

309

310

311

312

313

314

315

316

317

318

319

320

321

322

323

324

As a whole, the simulation of surface currents is worse than that in other layers, since winds and waves were not included in our MD2 model simulations, in which the surface flow is more susceptible to these forcings. The specified river flow at River 2 was constant, which may deviate from the real-time data (not available), leading to a poor salinity reproduction at upstream stations. In short, the water level and current are well-validated. The simulation of salinity is generally good, except for some deviations at upstream stations. It shows that the model can reasonably simulate the hydrodynamic processes in the area, and can be used for the following hydrodynamics study in the HE.

3. Results

3.1 Morphological evolution

Morphological changes between 1977, 1994, 2003, and 2010 are shown in Figs. 2a-c. ~~According to the pattern of erosion and siltation in the two consecutive years,~~ Figure 2a shows that most areas in the HE experienced siltation from 1977 to 1994, ~~but~~ the East Channel was deepened by about 0-0.5 m. In the middle of the bay, the nearshore areas were under erosion, and the erosion thickness at the eastern shore was twice that at the western shore. In other areas, the siltation thickness was between 0 and 0.5 m. From 1994 to 2003, erosion occurred in the West Shoal, East Channel, East Shoal, and Middle Shoal. Siltation of 0.01-0.5 m happened in the rest of the area, which accounted for most of the HE, so the HE became shallower in 2003. In 2003, siltation in the East Channel was serious and the water depth there became only 2m (Li, 2019). From 2003 to 2010, the West Shoal became significantly shallower with a siltation thickness of about 0.5-1m. The East Shoal almost disappeared, and its relict area endured siltation of 1.1-1.7 m, which was mainly due to the construction of coastal

325 protection works. Strong erosion occurred in other areas, especially in the upper bay
326 with a deepening of more than 4m, and the overall water depth of the HE became greater
327 in 2010. Relevant research shows that the East Channel had been under erosion from
328 2005 on and the largest water depth reached 7.4 m in 2006 (Luo, 2010).

329 ~~We further take the morphological change of the East Channel as an example. The~~
330 ~~East Channel experienced continuous erosion before 1977. From 1977 to 2003, the~~
331 ~~channel was under siltation, particularly at the river mouth bar (between the upper bay~~
332 ~~and the entrances, see Gong et al. (2014), whereas at the upper bay (from the head to~~
333 ~~the null point of the East Channel, here the null point means the convergence point at~~
334 ~~which the upstream seaward flow meets the downstream landward bottom flow) and at~~
335 ~~the inter-island sections, the channel was under erosion. In 2003, siltation in the East~~
336 ~~Channel was serious and the water depth there became only 2m (Li, 2019). From 2005~~
337 ~~on, the East Channel had been under erosion and the largest water depth reached 7.4 m~~
338 ~~in 2006 (Luo, 2010).~~

339 Overall, the water depth of the HE changed considerably from 1977 to 2010. It
340 first experienced erosion, then underwent siltation, and followed by erosion again.

341 Figure 2d shows the changes of coastlines for the four representative years. To
342 calculate the rate of geometry convergence, the DSAS tool (Version 5.0) in Arcmap
343 10.3 was used to calculate the end-point rates for cross-shore transects. A more detailed
344 procedure is in Zhang et al. (2019). We chose one longitudinal section along the channel
345 in the estuary and two cross-sections (in Fig. 2d) along the channel for analysis. The
346 longitudinal section (Sec. A) extends from the bay head (point A in Fig. 1b) to the
347 estuary mouth (point B in Fig. 1b), spanning a distance of 50 km. Sec. B1 is located at
348 about 4 km downstream from the bayhead, where the water depth changes sharply in
349 the lateral (or longitudinal) direction (see Fig. 2e). Sec. B2 is approximately 24km
350 downstream from the bayhead and near the null point in the middle of the estuary (see
351 Fig. 2f), and the width of the estuary varied dramatically here (see Fig. 2e). At Sec. A,
352 the water depth near the point of Sec. B1 endured a great change in 2010 due to channel
353 dredging (Fig. 2g). In other periods, the water depth along its course endured gradual

354 deepening. At Sec. B1, the bathymetric change is featured by an increase in water depth
355 and negligible change in width over time. At Sec. B2, both the water depth and width
356 experienced changes from 1977 to 2010, with the depth increased and width decreased
357 (Fig. 2f). The above three sections clearly depict the topographic changes of the estuary
358 in different years.

359

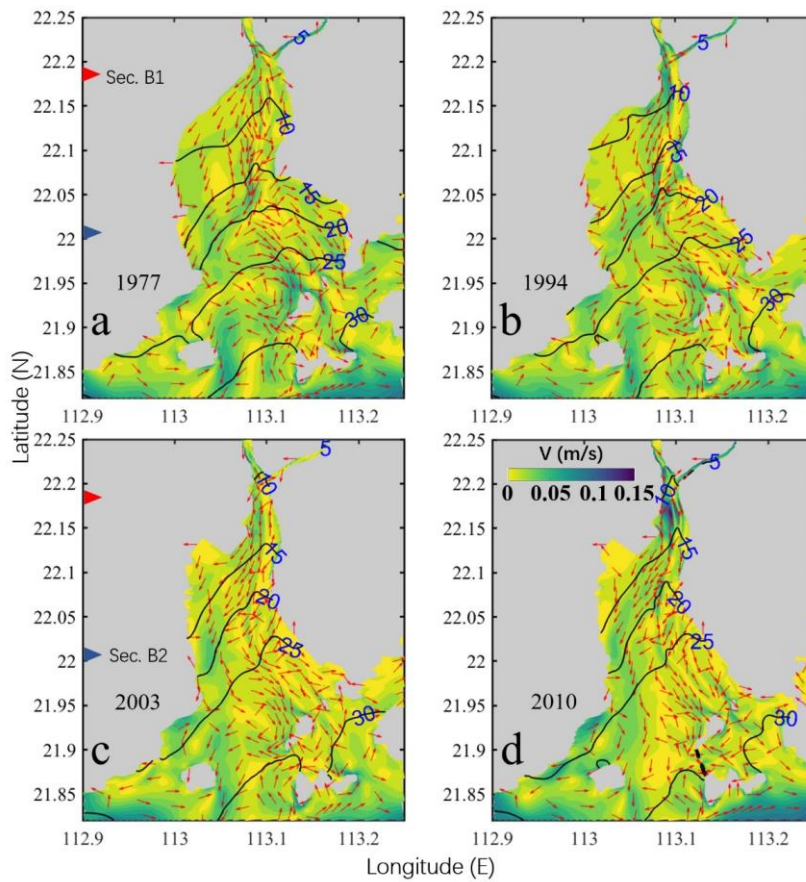
360 **3.2 Changes in the vertically averaged flow and salinity**

361

362 Here we present the changes in the tidally and vertically averaged flow and salinity
363 during neap tides ~~in different years~~ in Fig. 3. In 1977 (Fig. 3a), the current speed was
364 generally small, except at the inter-island sections and in the channel. The vertically
365 averaged flow was seaward in the upper bay and the right part of the lower bay (looking
366 landward). It became landward at the left part of the lower bay. ~~The 10 psu isohaline~~
367 ~~intruded into the upper bay at a latitude of 22.1 to 22.15°N.~~ In 1994 (Fig. 3b), the current
368 speed was increased in the channel, particularly near Sec.B1. The overall flow pattern
369 was almost similar to that in 1977. ~~The salt intrusion was increased, as the 10 psu~~
370 ~~isohaline intruded to a latitude of 22.15°N.~~ In 2003 (Fig. 3c), the flow pattern still kept
371 unchanged when compared to that in previous ~~periods~~ years. The current speed was
372 decreased relative to that in 1994. ~~However, the salt intrusion became aggravated as the~~
373 ~~10 psu isohaline had reached the bayhead at the Yamen Outlet.~~ In 2010 (Fig. 3d), the
374 seaward flow became more dominant in the upper bay, and more biased southwestward.
375 The seaward flow in the channel was greater than in 2003. ~~The 10 psu isohaline kept~~
376 ~~moving upstream over time. The salt intrusion was more serious than in 2003, as and~~
377 ~~the 10 psu isohaline~~ reached beyond the bayhead and entered into the tidal river of the
378 estuary in 2010.

379 Overall, we observed that the tidally and vertically averaged flow during neap tides
380 experienced an increase-decrease-increase by the topographic changes, whereas the
381 saltwater consistently intruded ~~further into the estuary~~ more landward.

382 As a supplement, we present the horizontal distributions of tidally averaged
 383 surface and bottom circulation and salinity during neap tides for different years in the
 384 appendix (Figs. A. 5-1 and 62). Over the study period, the enhancement of salt intrusion
 385 was stronger for the bottom layer and weaker for the surface layer, whereas the increase
 386 in residual flow was stronger in the surface layer and weaker in the bottom layer.



387
 388 Fig. 3. Patterns of the vertical-averaged horizontal circulation during neap tide in 1977(a1),
 389 1994(a2), 2003(a3), and 2004(a4). The magnitude of the current is represented by the color
 390 shading, while the current direction is shown by the arrows. The salinity is depicted by the
 391 contour lines. The red and blue triangles depict the positions of two cross-sections (Sec.B1 and
 392 Sec.B2).

393

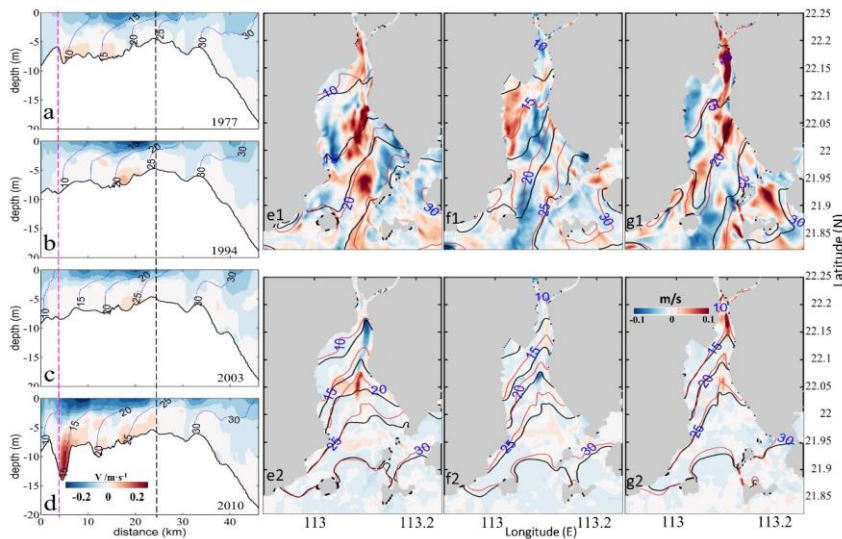
394 3.3 Changes in the estuarine circulation

395

396 Figures 4 a-d ~~present the longitudinal estuarine circulation and the distributions of~~
397 ~~salinity isolines during the neap tide in the longitudinal section (Sec. A in Fig. 1b) in~~
398 ~~different years. The results~~ show that the upper part of the estuary (upstream of the null
399 point) was highly stratified, and the lower part of the estuary (downstream of the null
400 point) was well mixed. The classical exchange flow structure of ~~“a landward residual~~
401 ~~flow near the bottom and a seaward residual flow near the surface”~~ was more distinct
402 upstream of the null point. Over time, the surface seaward flow became stronger and
403 more concentrated with the narrowing of the estuary, particularly in 2010. It extended
404 more downstream to near the estuary mouth with the narrowing of the estuary, as
405 evidenced by the extent of the seaward flow of 0.2 m/s. Concomitantly, the bottom
406 landward flow was strengthened and concentrated with the increase in depth. It should
407 be noted that the greatly enhanced estuarine circulation between 3 to 8 km in 2010 (Fig.
408 4d) could be induced by the intratidal fluctuation of the halocline in response to the
409 large topography change there(Geyer and Nepf, 1996; Chen et al., 2012; Wang et al.,
410 2015)

411 We also present the changes in the surface and bottom current horizontally. Figs.
412 4e1-g1 show that when the estuary deepened (1977-1994 and 2003-2010), the surface
413 current ~~speed-velocity~~ increased in the channel, and when the estuary shoaled (1994-
414 2003), the surface current velocity in the channel decreased. The changes in the bottom
415 current showed a similar trend (Figs. 4e2-g2), except at the upper part of the channel
416 from 1977 to 1994, in which the width was considerably ~~narrowed~~ decreased.

417 Along with the change in the longitudinal estuarine circulation, the salt intrusion
418 at Sec. A did not change significantly from 1977 to 1994, but increased from 2003 on,
419 particularly in 2010, when the isohaline of 15 psu reached Sec.B1, whose salinities
420 were less than 12 psu in previous years (Figs. 4a-d). The salt intrusions at the surface
421 and bottom gradually increased with the estuary narrowing (Figs. 4e1-g2).



422

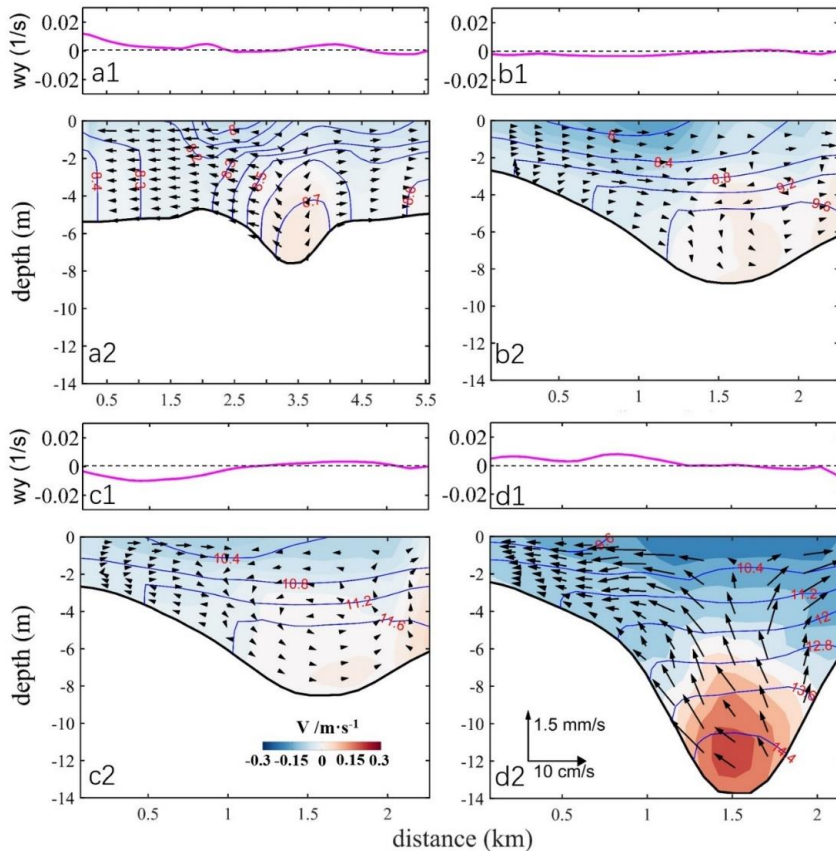
423 Fig. 4. The patterns of the estuarine circulation during the neap tide in March 1977(a), 1994(b),
 424 2003(c), and 2010(d). The thin lines are the isolines of salinity in a-d. The pink and black dotted
 425 lines represent the locations of Secs. B1 and B2, respectively. The starting point of the X-axis
 426 is Point A in Fig. 1b. Surface current differences from 1977 to 1994(e1), from 1994 to 2003(f1),
 427 and from 2003 to 2010(g1); Bottom current differences from 1977 to 1994(e2), from 1994 to 2003
 428 (f2), and from 2003 to 2010(g2). The red and black lines represent the isolines of salinity
 429 in the later year and the earlier year.

430

431 To analyze the changes of lateral circulation in the estuary, we show the structure
 432 and intensity of the lateral circulation at the two cross-sections (Figs. 5 and 6).

433 At Sec. B1 (Fig. 5), with the increase of water depth, the salinity difference
 434 between the surface and bottom increased, along with an increase in the bottom salinity,
 435 which is more than 14 psu in 2010. For the lateral circulation, there was no distinct gyre
 436 structure in 1977, but a pair of opposite vortices started to develop at the position of
 437 3.5km. In 1994, the lateral flow was dominated by an eastward flow. In 2003, a
 438 clockwise vortex was developed over the West Shoal (0.5-1 km). Meanwhile, an
 439 anticlockwise circulation with smaller vortex intensity was developed in the region of
 440 1-2km from the western shore. Another clockwise circulation was developed over the
 441 East Shoal. When the estuary became deepened in 2010, the distribution of the lateral

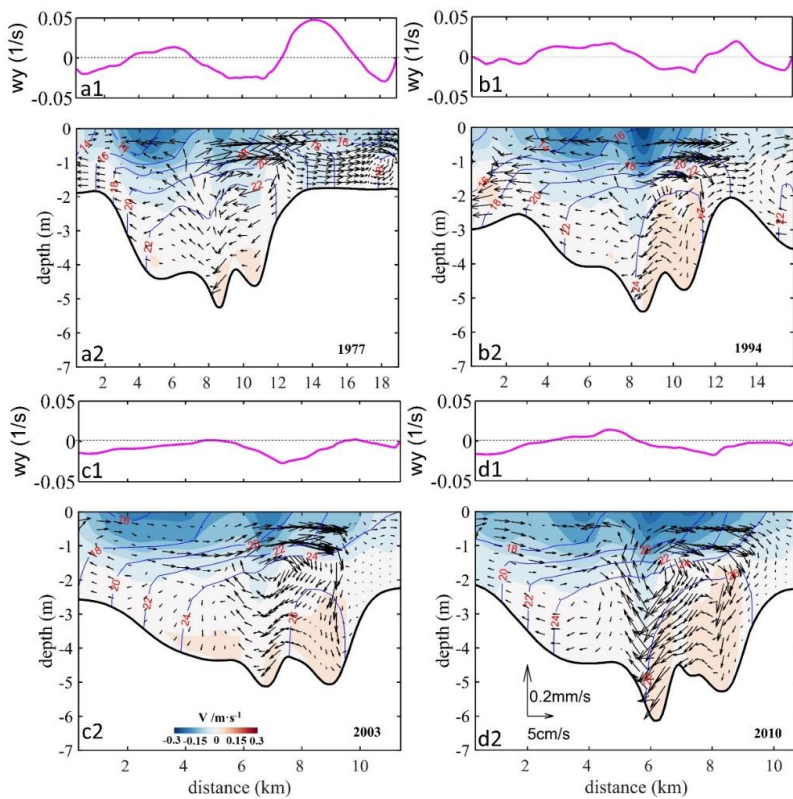
442 circulation was similar to that in 1977, but the vortex intensity increased significantly
 443 to about 2-4 times that of 1977.



444
 445 Fig. 5. The lateral circulation and isohalines (blue lines) at Sec. B1 in 1977(a2), 1994(b2),
 446 2003(c2), and 2010(d2). The starting point of the X-axis is Point C in Fig. 2d. w_y is the
 447 longitudinal vorticity at Sec. B1 in 1977(a1), 1994(a2), 2003(a3), and 2010(a4).

448
 449 Figure 6 shows the changes in lateral circulation at Sec. B2. With the decrease of
 450 estuary width, the salinity increased in the cross-section over the years. There
 451 developed a clockwise circulation at the right of the deep channel in 1977 and 1994.
 452 This clockwise vortex was seen to move westward from 2003 on. The spatial extent of
 453 the clockwise circulation in the deep channel increased significantly over time.
 454 Clockwise vortices developed over the East Shore from 1977 to 2010, but their intensity

455 became weaker since 2003. In 1977 and 1994, the distance between the deep channel
 456 and the East Shore was greater than 2 km ~~that which was sufficient enough for~~
 457 ~~accommodating developing clockwise vortices, and the accommodation space was~~
 458 ~~enough for the clockwise vortices to develop sufficiently.~~ From 2003 on, the
 459 accommodation space at the East Shore became limited and restricted the full
 460 development of the clockwise vortex. Over the West Shoal, the lateral circulation
 461 pattern showed an anticlockwise circulation in 1977 and 1994. However, since 2003,
 462 the lateral circulation over the West Shoal began to develop a two-cell pattern, with an
 463 anticlockwise gyre at the surface and a clockwise one near the bottom. The clockwise
 464 cell developed well in 2010.



465
 466 Fig. 6. The distribution of lateral circulation and isohalines (blue lines) at Sec.B2 in 1977(a2),
 467 1994(b2), 2003(c2), and 2010(d2). The starting point of the X-axis is Point E in Fig. 2d. w_y
 468 is the longitudinal vorticity at Sec. B2 in 1977(a1), 1994(a2), 2003(a3), and 2010(a4).

469

470 As a whole, over the study period, the longitudinal estuarine circulation continued
471 to increase, whereas the lateral circulation experienced varying changes at different
472 cross-sections. At the upstream cross-section (B1), when the estuary narrowed, the
473 original pattern of two-cell vortices with opposite polarity was disrupted. However, it
474 was amplified in 2010 when the water depth was increased. At the cross-section in the
475 middle of the estuary (B2), a similar two-cell pattern was developed. However, in 2003
476 and 2010, the single cell at the West Shoal was split into two cells: an anticlockwise
477 cell at the surface and a clockwise cell at the lower part.

478

479 **3.4 Relationship between the ~~g~~Changes in the intensity of estuarine circulation** 480 **and the changes in topography**

481

482 To further quantitatively identify the influence of topographic changes on the
483 estuarine circulation, we calculated the changes in the intensity of estuarine circulations
484 in the longitudinal and lateral directions. The magnitude of estuarine circulation in the
485 longitudinal section was used to represent the intensity of the longitudinal estuarine
486 circulation (Chen and Sanford, 2009). The method was to subtract the subtidal
487 longitudinal velocity of the bottom layer from that on the surface layer. The magnitude
488 of the vorticity in the cross-sections was used to represent the intensity of the lateral
489 circulation (Becherer et al. 2015), and is expressed as:

$$490 \quad w_y = \partial w / \partial x - \partial u / \partial z \quad (2)$$

491 where, w_y is the longitudinal vorticity in the cross-sections. w and u are the
492 currents in the vertical and lateral directions, respectively. $\partial w / \partial x$ is much smaller
493 and can be ignored, therefore, ~~the formula (2) for calculating the intensity of lateral~~
494 ~~circulation~~ can be simplified as:

$$495 \quad w_y = -\partial u / \partial z \quad (3)$$

496 when w_y is positive, the lateral circulation is an anticlockwise vortex, conversely,

497 when w_y is negative, the lateral circulation is a clockwise vortex.

498 The results of the averaged intensity of estuarine circulation along ~~Sec.A the~~
 499 ~~longitudinal section~~ and the averaged intensity of vorticity at the cross-sections are
 500 listed in Table 4.

501
 502 Table 4. The changes of width and depth (the maximum depth), area (cross-section area), w-to-
 503 d, narrowing rate, deepening rate, and the intensity of circulations (w-to-d: width-to-depth ratio;
 504 narrowing rate: the ratio of the difference of cross-section widths between two years divided
 505 by the width in the earlier year; deepening rate: the ratio of the difference of water depth in the
 506 cross-section between the corresponding two years divided by the earlier depth. The positive
 507 narrowing rate indicates that the estuary is narrowed; the positive deepening rate indicates that
 508 the estuary is deepened.)

509

		time	1977/03	1994/03	2003/03	2010/03
Sec.B1	width (km)		5.56	2.25	2.26	2.14
	depth (m)		7.58	8.76	8.50	13.73
	w-to-d		734	257	266	156
	area (km ²)		0.0468	0.0213	0.0207	0.0256
	narrowing rate		\	59.50%	-0.44%	5.30%
	deepening rate		\	15.58%	-2.95%	61.47%
Sec.B2	width (km)		18.97	15.77	11.40	10.76
	depth (m)		5.25	5.40	5.12	6.13
	w-to-d		3610	2920	2230	1760
	area (km ²)		0.0849	0.303	0.0647	0.0646
	narrowing rate		\	16.87%	27.71%	5.61%
	deepening rate		\	2.86%	-5.19%	19.73%
circulation intensity	longitudinal	Sec. A	0.0274	0.0428	0.0483	0.0594
	lateral	Sec. B1	0.0111	0.0146	0.0130	0.0278
		Sec. B2	0.0493	0.0460	0.0465	0.0425

510

511 Table 4 indicates that the longitudinal estuarine circulation intensity increased with
 512 the estuary narrowing, and reached the largest in 2010, which was 0.0594 m/s.

513 The lateral circulation intensity varied in different cross-sections. For Sec.B1, it
 514 increased gradually when the estuary deepened (from 1994 to 2010). When the
 515 deepening rate reached the maximum (61.47%) in 2010, the lateral circulation intensity
 516 reached the maximum as well. The intensity of lateral circulation increased when the
 517 estuary deepened and narrowed (from 1977 to 1994, and from 2003 to 2010), but it
 518 decreased when the estuary shallowed and narrowed (from 1994 to 2003). For Sec.B2,

519 the intensity of lateral circulation decreased when the estuary deepened and narrowed
 520 (from 1977 to 1994, and from 2003 to 2010). However, this trend was altered when the
 521 estuary entered into the “narrowing and shallowing period”, with the deepening rate
 522 being -5.19%. ~~The lateral circulation intensity increased in 2003. The change in the~~
 523 ~~lateral circulation intensity~~—It indicates that changes in water depth were the dominant
 524 factors affecting the lateral circulation intensity.

525 In general, the relationship between the longitudinal estuarine circulation intensity
 526 and the estuary width showed a monotonic decrease, while that between the
 527 longitudinal estuarine circulation intensity and the water depth is a monotonic increase,
 528 but the lateral circulation intensity seemed to have no simple linear relationship with
 529 the topographic change. ~~including changes in the estuary width, water depth, and cross-~~
 530 ~~section area.~~

531

532 4. Discussion

533

534 4.1 Contribution of momentum terms to the variation of the longitudinal 535 estuarine circulation

536

537 To explain the change in the longitudinal estuarine circulation intensity, we
 538 conducted a diagnostic study by examining the changes in terms of the momentum
 539 balance equations. We calculated each term of the momentum equation in the
 540 longitudinal direction in the tidally averaged timescale:

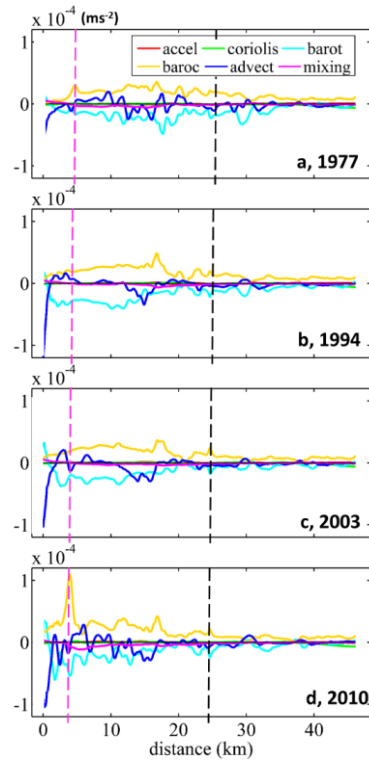
$$541 \frac{\partial v}{\partial t} = \underbrace{fu}_{\text{coriolis}} - \underbrace{g \frac{\partial \eta}{\partial y}}_{\text{barotropic pressure}} - \underbrace{\frac{gz}{\rho_0} \frac{\partial \rho}{\partial y}}_{\text{baroclinic pressure}} - \underbrace{\left(u \frac{\partial v}{\partial x} + v \frac{\partial v}{\partial y} + w \frac{\partial v}{\partial z} \right)}_{\text{advection}} + \underbrace{\frac{\partial}{\partial z} \left(A_v \frac{\partial v}{\partial z} \right)}_{\text{vertical friction}}, \quad (4)$$

542 By comparing the changes in each term and linking them with the characteristics
 543 of morphological evolution, we ~~try effort~~ to explain the response of the longitudinal
 544 estuarine circulation to bathymetric change in the perspective of momentum balance.
 545 Though the change in an individual momentum term in Eq. 4 can not represent the
 546 change in the longitudinal estuarine circulation as a whole, it can reflect the change in
 547 the corresponding component for the estuarine circulation (Cheng, 2013). For example,

548 an increase or decrease in the baroclinic pressure gradient force can reflect the change
549 in the gravitational circulation, and the change in the advection term is representative
550 of the change in tidal rectification. In the following, we present ~~both~~ the vertically
551 averaged ~~and depth dependent~~ values for these different terms along the longitudinal
552 section in different years. It should be noted that the friction term consists of a
553 component of the tidally mean eddy viscosity multiplied by the tidally mean vertical
554 current shear, and a component of the correlation between eddy viscosity and vertical
555 current shear, which is referred to as the tidal straining (Simpson et al., 1990).

556 Figure 7 shows that during the neap tide, the baroclinic pressure gradient force
557 was balanced by barotropic gradient force, friction, and advection term in each year.
558 This is different from the classic estuarine momentum balance (Pritchard, 1956) but
559 consistent with the recent understanding of estuarine physics (Geyer and MacCready,
560 2014). The Coriolis force is quite small as both the latitude of the HE and the residual
561 current are small. The high value of the baroclinic term was observed to shift upstream
562 over time. As the baroclinic term is the multiplication of the salinity gradient and water
563 depth, the changes in this term over years can be induced by the change in water depth
564 and/or the salinity gradient. It can be seen from Fig. 4 that in the north of the null point,
565 the salt intrusion gradually moved towards the bayhead with the estuary narrowing,
566 thus increasing the salinity gradient there. In the meantime, the upstream water depth
567 was increased due to channel dredging, particularly in 2010. Therefore, the increase of
568 the baroclinic force term was caused by both the increases in water depth and salinity
569 gradient. Although the barotropic term contributed a lot to the momentum balance, it
570 did not change obviously with the morphological evolution. The advection term at the
571 upstream section (B1) increased slightly with the estuary narrowing, especially in the
572 deepening part of the channel in 2010. The friction term at the upstream section (B1)
573 was the largest in 2010, because the salt intrusion increased the vertical shear of the
574 longitudinal current there. Nevertheless, the increase in friction term was much smaller
575 than that of the baroclinic term. Chant et al. (2018) attributed the increase in exchange
576 flow to the increase in horizontal salinity gradient and/or a reduction in vertical mixing

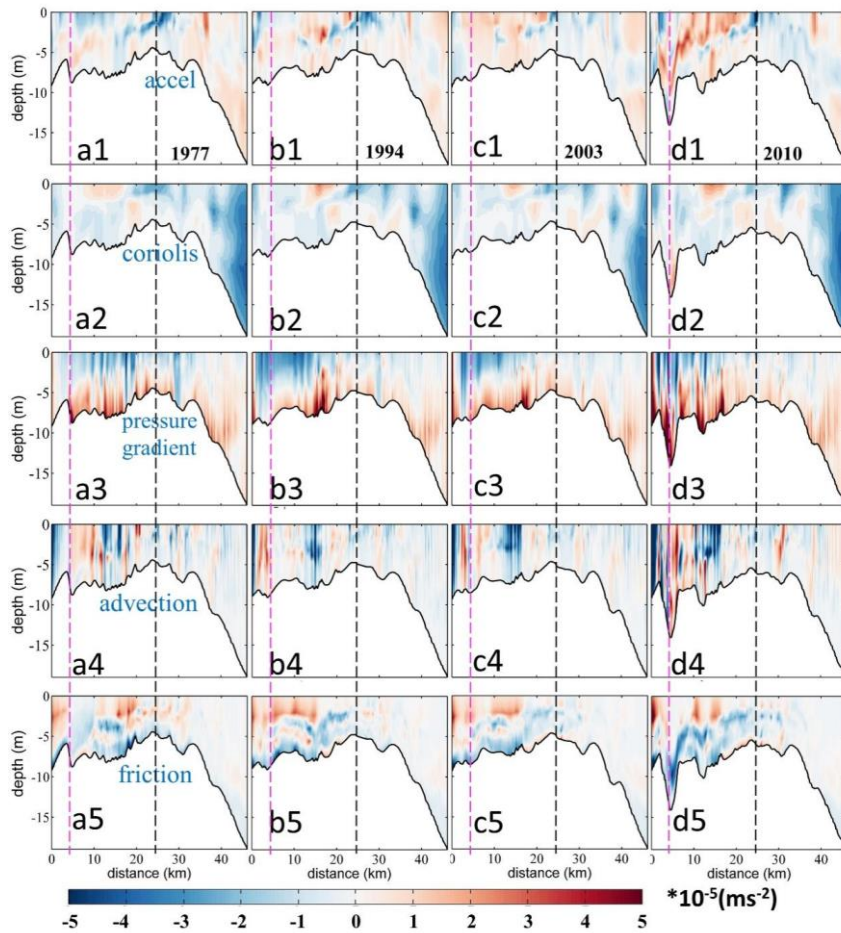
577 by deepening, but in our case, the increase in baroclinic term was dominant and the
 578 change in vertical mixing even posed a reversed effect.



579 Fig. 7. Patterns of the longitudinal momentum terms during neap tide at Sec. A in 1977(a),
 580 1994(b), 2003(c), and 2010(d). The starting point of the X-axis is Point A in Fig. 1b. “accel” in
 581 legend: local acceleration term; “barot” in legend: the barotropic gradient force term; “baroc”
 582 in legend: the baroclinic gradient force.
 583

584
 585 **In Fig.8, we present the distribution of each momentum term in the longitudinal**
 586 **section and its change with the morphological evolution. Among them, the distribution**
 587 **patterns in 1994 and 2003 were very similar. The area of maximum bottom landward**
 588 **pressure gradient force was shifted to the upper bay. The magnitudes of the bottom**
 589 **pressure gradient force in 1994 and 2003 were greater than that in 1977, but less than**
 590 **that in 2010. The advection term alternated between positive and negative along Sec.**
 591 **A, and was increased in the upper part of Sec. A in 2010. The friction term generally**

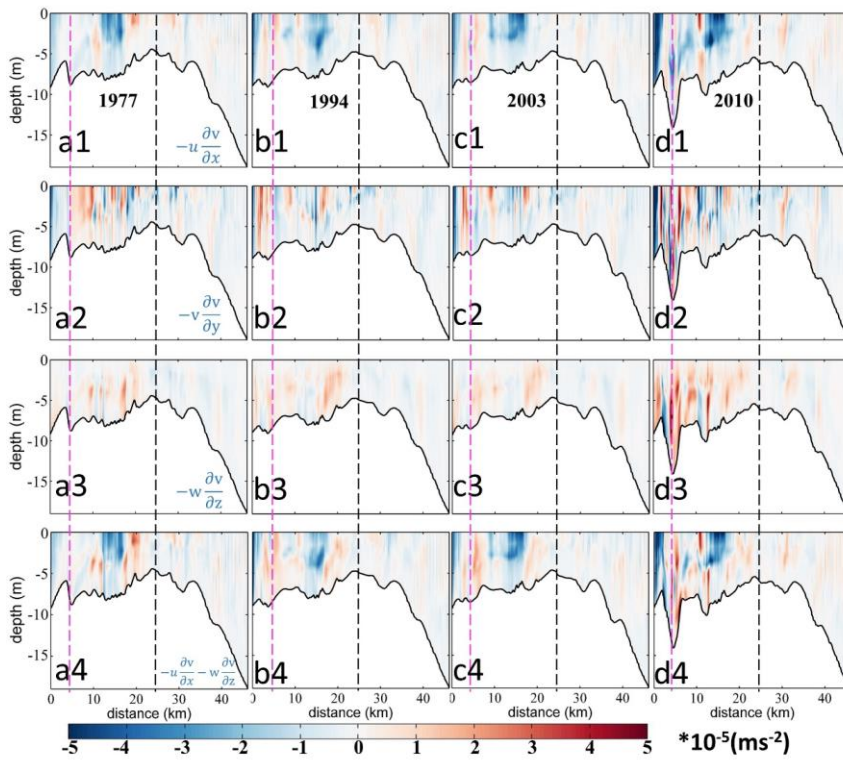
592 shows a pattern of positive in the upper part and negative in the lower part of the water
 593 column, opposite to the estuarine circulation. In the region where the seaward flow was
 594 dominant in the whole water column (around 30 km), the friction was positive near the
 595 bottom. It can be seen that near Sec. B1, the friction at the bottom increased in 2010,
 596 showing an increase in the bottom landward flow.—



597
 598 Fig. 8. Patterns of the longitudinal momentum terms during neap tide at Sec. A. (a1 d1): The
 599 local acceleration term. (a2 d2): The Coriolis term. (a3 d3): The pressure gradient force term.
 600 (a4 d4): The advection term. (a5 d5): The friction (vertical mixing term). 1977, 1994, 2003,
 601 and 2010 cases are in the first, second, third, and fourth columns, respectively. The pink and
 602 black dotted lines represent the location of Sec.B1 and Sec.B2, respectively. The starting point

603 of the X-axis is Point A in Fig. 1b. For viewing purposes, the acceleration term is multiplied by
 604 10.

605 To further identify the changes in different terms, the advection term was divided
 606 into lateral (X-direction), longitudinal (Y-direction), and vertical (Z-direction)
 607 advection terms (Fig. 98). The It is worth noting that the sum of the advection terms in
 608 X and Z directions represents the effect of the lateral circulation. The lateral and
 609 longitudinal advection terms are collectively referred to as the horizontal advection
 610 term.



611
 612 Fig. 98. Patterns of the longitudinal momentum terms during neap tide at Sec. A. (a1-d1): The
 613 advection in the X direction, $-u \frac{\partial v}{\partial x}$. (a2-d2): The advection in the Y direction, $-v \frac{\partial v}{\partial y}$. (a3-d3):
 614 The advection in the Z direction, $-w \frac{\partial v}{\partial z}$. (a4-d4): The sum of the advection terms in X and Z
 615 directions. 1977, 1994, 2003, and 2010 cases are in the first, second, third, and fourth columns,

616 respectively. The pink and black dotted lines represent the location of Sec.B1 and Sec.B2,
 617 respectively. The starting point of the X-axis is Point A in Fig. 1b.

618
 619 From Fig. 98, in 2010, the advection terms in all directions increased significantly.
 620 Generally, the lateral and vertical advection competes against each other, and their
 621 additive effect is to generate a circulation similar to the gravitational circulation. This
 622 effect was the strongest in 2010 (Figs. 9a4_8a4-d4). The longitudinal advection
 623 increased in the upper part of the channel in 2010 (Figs. 9a28a2-d2), following the
 624 deepening and narrowing of the estuary. In the middle of the longitudinal section, it
 625 induced a seaward flow at the surface and a landward flow at the bottom, whereas at
 626 the upper part, it generates a uniformly landward flow.

627 ~~Therefore, the maximum longitudinal estuarine circulation in 2010 was caused by~~
 628 ~~the increase in the pressure gradient force and the advection term, especially the~~
 629 ~~baroclinic pressure gradient force. The largest variation of the advection and pressure~~
 630 ~~gradient terms occurred in the period of topography narrowing and deepening.~~

631 Overall, from 1977 to 2010, the baroclinic force, the friction, and the advection
 632 terms were seen to increase along the Sec. A. ~~The maximum longitudinal estuarine~~
 633 ~~circulation in 2010 was caused by the increase in the pressure gradient force and the~~
 634 ~~advection term, especially the baroclinic pressure gradient force.~~ We will further
 635 discuss the effects of these changes on estuarine circulation.

636

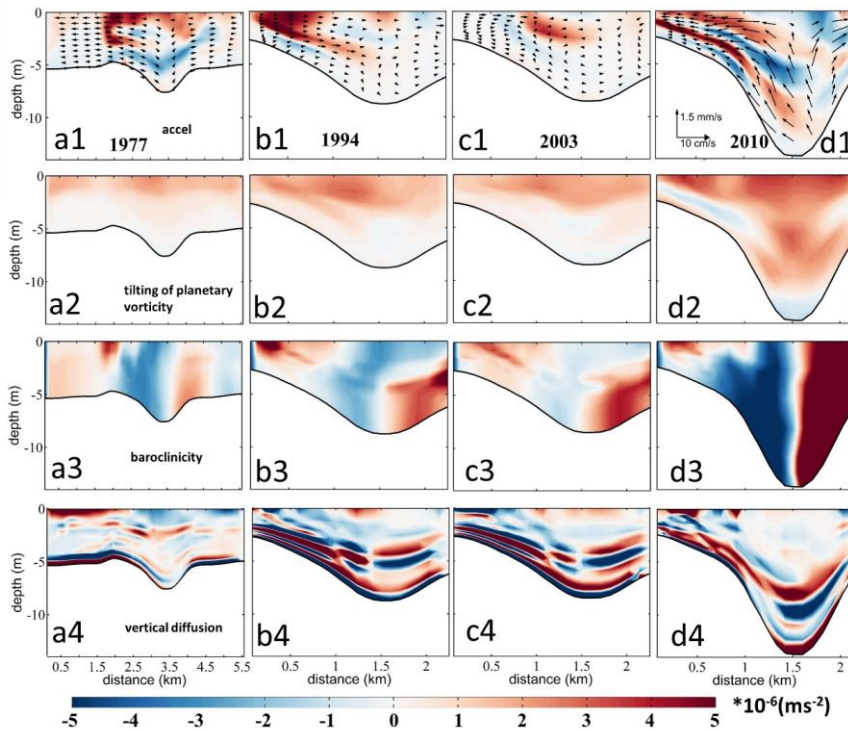
637 4.2 Analysis of the streamwise vorticity balance for the lateral flow

638

639 In order to reveal the contribution of the vertical shear of the along-channel flow,
 640 the lateral salinity gradient, and the vertical diffusion to changes in the lateral
 641 circulation, we examine the changes in terms of the streamwise vorticity transport
 642 equation (Li et al., 2014):

643
$$\frac{dw_y}{dt} = \underbrace{-f \frac{\partial v}{\partial z}}_{\text{tilting of planetary vorticity}} \underbrace{-g\beta \frac{\partial s}{\partial x}}_{\text{baroclinicity}} + \underbrace{\frac{\partial^2}{\partial z^2} (K_V w_y)}_{\text{vertical diffusion}} + \underbrace{\frac{\partial^2}{\partial x^2} (K_H w_y)}_{\text{horizontal diffusion}}, \quad (5)$$

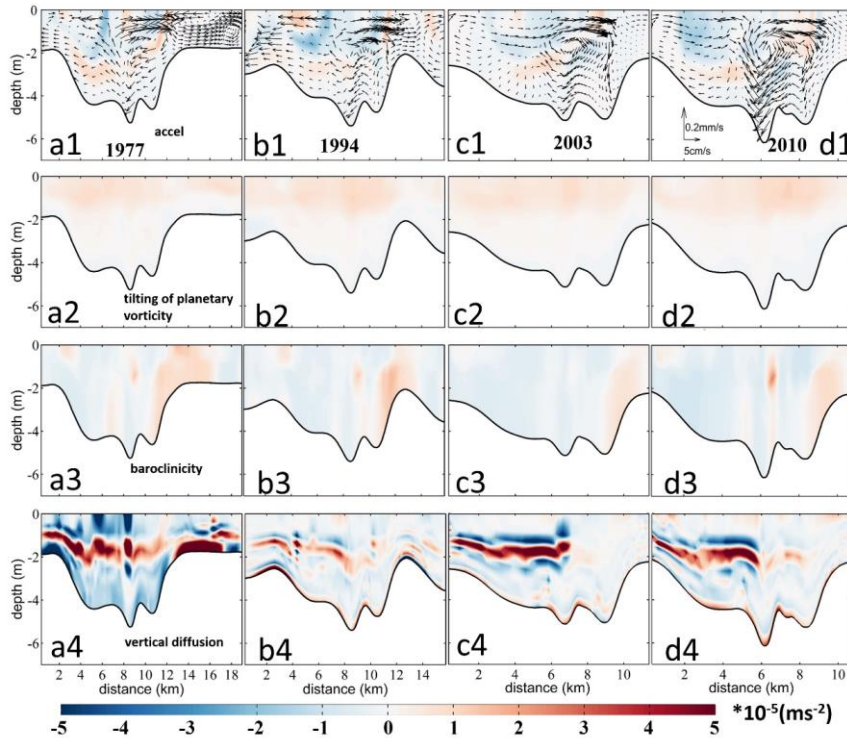
644 In the right side of Eq. 5, the first term represents the tilting of the planetary
 645 vorticity by vertical shear in the along-channel flow, the second term is the baroclinicity
 646 caused by the lateral salinity gradient, the third is the vertical diffusion, and the fourth
 647 is the horizontal diffusion, which is typically two orders of magnitude smaller than the
 648 vertical diffusion term. Therefore, we only show the first four terms in Fig. 109.



649 Fig. 109. Patterns of the streamwise vorticity equation terms during neap tide at Sec. B1. (a1-
 650 d1): The local acceleration term. (a2-d2): The tilting of planetary vorticity term. (a3-d3): The
 651 baroclinicity term. (a4-d4): The vertical diffusion term. The cases in 1977, 1994, 2003, and
 652 2010 are in the first, second, third, and fourth columns, respectively. The starting point of the
 653 X-axis is Point C in Fig. 2d. For viewing purposes, the acceleration term is multiplied by 5. The
 654 block arrows in a1-d1 represent the distribution of lateral circulation.
 655
 656

657 Figure 109 shows that the changes of baroclinicity terms caused by the water depth
 658 change dominated the changes in the lateral circulation at Sec. B1. The baroclinicity
 659 term in the deep channel was generally negative at the left side of the channel, and it

660 increased significantly in 2010, about 2-3 times the value in 1977. The baroclinicity
661 term with positive values occurred ~~over~~at the West Shoal over the study period, but the
662 areal extent occupied by the positive values decreased gradually, with its magnitude
663 increased obviously in 1994 when the narrowing rate was the largest. A negative
664 baroclinicity term appeared at the bottom of the West Shoal, indicating that the changes
665 in water depth can lead to changes in the pattern and magnitude of the baroclinicity
666 term, which was mainly caused by the changes in the salt intrusion. The tilting of the
667 planetary vorticity term increased with the estuary narrowing, with the increase ~~of this~~
668 ~~term~~ in 2010 was greater, which was mostly caused by the depth change. The pattern
669 of the vertical diffusion term changed significantly in 1977 and 1994. ~~It changed~~,
670 especially at the surface and the bottom layers of the West Shoal. ~~When the width~~
671 ~~decreased to about 2.5 km, the distribution of vertical diffusion was reversed compared~~
672 ~~with 1977~~, indicating that it was the changes in width that altered the vertical diffusion
673 term.



674
 675 Fig. 4+10. Patterns of the streamwise vorticity equation terms during neap tide at Sec. B2. (a1-
 676 d1): The local acceleration term. (a2-d2): The tilting of planetary vorticity term. (a3-d3): The
 677 baroclinicity term. (a4-d4): The vertical diffusion term. The cases in 1977, 1994, 2003, and
 678 2010 are in the first, second, third, and fourth columns, respectively. The starting point of the
 679 X-axis is Point E in Fig. 2d. For viewing purposes, the acceleration term is multiplied by 5. The
 680 block arrows in a1-d1 represent the distribution of lateral circulation.

681 From Fig. 4+10, the change in the tilting of the planetary vorticity at Sec. B2 was
 682 analogous to that at Sec. B1. The baroclinicity term did not change much, because the
 683 changes in water depth were smaller in this section than that at Sec. B1. The clockwise
 684 circulation over the West shoal increased as the estuary deepened in 2010, because the
 685 baroclinicity term was larger with the increase of salt intrusion and vertical salinity
 686 gradient near Sec. B2. The vertical diffusion of the vorticity was overall negative,
 687 indicating its effect in dissipating the vorticity. The vertical diffusion term was larger
 688 than the baroclinicity term, especially in the middle water, which was inconsistent with
 689 the conclusion that the baroclinicity term is the most important one in the lateral

690 circulation (Li et al., 2014). The reason may be that in our study site, the vertical mixing
691 was strong as the estuary became shallow. However, the existence of a pycnocline
692 greatly weakened the momentum exchange between the upper and lower layers: above
693 the pycnocline, the tilting of the planetary vorticity was dominant; whereas, under the
694 pycnocline, the baroclinic term was dominant. The decrease of the estuary width
695 changed the magnitude and pattern of the vertical diffusion term, ~~especially when the~~
696 ~~estuary width was less than 15 km, and~~ the area with a large positive value at the bottom
697 of the East Shoal disappeared, ~~and along with~~ the magnitude of the negative value
698 decreased greatly at the easternmost of the section. It indicates that in a shallow estuary,
699 the vertical diffusion term caused by the width change is also important.

700 In Summary, the tilting of the planetary vorticity increased with the decrease of
701 width or with the increase of water depth. The variation of estuary width was
702 responsible for the changes in the vertical diffusion term, and the changes in water depth
703 were responsible for the changes in the baroclinicity term. The increase of the
704 longitudinal estuary circulation can increase the baroclinicity term ~~of~~ at the cross-
705 sections by increasing the salinity gradient near the cross-sections, which mainly
706 occurred in the periods of the estuary deepening. The deepening rate of Sec.B1 was the
707 highest (61%) in 2010, which led to the strongest lateral circulation in 2010. The lateral
708 circulation intensity decreased when the estuary narrowed in 2003 due to the decreased
709 baroclinicity term. In addition, the shallowing was the main reason for the pattern
710 change of the lateral circulation at Sec.B2. At Sec. B2, the narrowing rate was the
711 largest in 2003, and the adjustment of the vertical diffusion term resulted in an increased
712 lateral circulation from 1994 to 2003. The decrease of the clockwise circulation at the
713 East Shoal was mainly related to the adjustment of the vertical diffusion term to the
714 baroclinicity term.

715

716 **4.3 Comparison to theoretical results and other estuaries influenced by human** 717 **interventions**

718

719 The longitudinal estuarine circulation is generated by the river discharge, Stokes
 720 return flow, longitudinal baroclinic pressure force, tidal straining, and advection (Geyer
 721 and Maccready, 2014). The HE features a microtidal tidal regime (tidal range less than
 722 1.5 m), and the component generated by the baroclinic pressure gradient, i.e., the
 723 gravitational circulation, would be a primary part of the longitudinal estuarine
 724 circulation. The convergent geometry makes it susceptible to the residual flow induced
 725 by the longitudinal advection (Burchard et al., 2014). However, as seen above, the
 726 horizontal advection also plays a role in generating the estuarine circulation.

727 With channel deepening and width narrowing in the HE, the gravitational
 728 circulation was increased by the increased baroclinic pressure gradient force. Based on
 729 Geyer's research (2010), the gravitational circulation ~~can be simplified as to: in a straight~~
 730 ~~estuary of rectangular cross section is scaled as:~~

$$731 \quad v_g = a(\beta g s_0 h)^{1/5} U_x^{1/5} U_t^{2/5} = a(\beta g s_0 h)^{1/5} R^{1/5} (wh)^{-1/5} U_x^{2/5}, \quad (6)$$

732 in which a is a constant, β is the salinity expansion coefficient, g is the gravity
 733 acceleration, s_0 is the oceanic salinity, R is the river discharge, w is the width of
 734 the cross-section, U_t is the tidal velocity amplitude, h is the water depth, U_x is the
 735 outflow velocity associated with the river discharge. Where $u_x = Q_x/A_{cs}$ (Q_x is the
 736 freshwater outflow, A_{cs} being the local cross-sectional area of the estuary).

737 If we simply assume that the change in tidal current amplitude follows the Green's
 738 law $U_t = U_0 \sqrt{\frac{w_0 h_0}{wh}}$ (here w_0 and h_0 is the width and depth at the estuary mouth,
 739 respectively), then the gravitational circulation becomes:

$$740 \quad v_g = a(\beta g s_0 h)^{1/5} R^{1/5} (wh)^{-1/5} U_0^{2/5} (w_0 h_0)^{1/5} (wh)^{-1/5}$$

$$741 \quad = a_1 (\beta g s_0 R w_0 h_0)^{1/5} U_0^{2/5} w^{-2/5} h^{-1/5}, \quad (76)$$

742 in which w_0 and h_0 is the width and depth at the estuary mouth, respectively.

743 It indicates that the gravitational circulation is inversely related to the water depth
 744 and width in the estuary, with a weaker dependence on the water depth. In Chant et al.
 745 (2018), the gravitational circulation is completely unrelated to the water depth in their

带格式的: 左, 缩进: 首行缩进: 0 字符

746 equation (2), which is $v_g \propto \left(\frac{g'R}{w}\right)^{\frac{1}{3}}$, in which the g' is the reduced gravity acceleration.

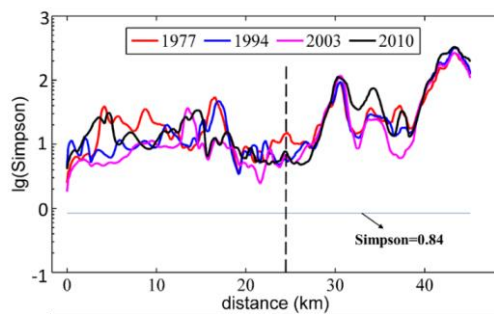
747 This seems to contradict the situations occurring in many estuaries, such as in the Coos
748 Bay (Eidam et al., 2020), Tampa Bay (Zhu et al., 2015), Changjiang Estuary (Zhu,
749 2018), Ems estuary (Van Maren et al., 2015), Hudson Estuary (Ralston and Geyer,
750 2019), and Newark Bay of the Delaware estuary (Chant et al., 2018). In all these
751 estuaries, the gravitational circulation demonstrated an increase with the deepening of
752 the channel. It suggests that the changes in gravitational circulation vary in different
753 parts of the estuary and the longitudinal salinity gradient may not catch up with the
754 change in water depth in the analytical solution, proposed by Chant et al. (2018) and
755 Ralston and Geyer (2019). In our study site, the salinity gradient at the upstream part
756 of the longitudinal section was increased owing to an enhanced salt intrusion where
757 water depth increased, which led to an increased gravitational circulation in the
758 upstream of the HE (Fig. 4).

759 The tidal straining-induced estuarine circulation is another important component of
760 longitudinal estuarine circulation. The straining-induced circulation is the covariance
761 of the eddy viscosity and the vertical shear of the longitudinal flow (ESCO) in a tidal
762 cycle and is included in the term of internal friction. Cheng et al. (2010) have indicated
763 that ESCO-induced flow dominates the gravitational circulation in periodically
764 stratified estuaries with strong tides, having the same structure as the gravitational
765 circulation. It has the same order of magnitude in weakly stratified estuaries with
766 moderate tides, and is less important in highly stratified estuaries with weak tides, even
767 with a reversed structure with the gravitational circulation. As indicated by Becherer et
768 al. (2015), the strength of the straining-induced circulation is dependent on the Simpson
769 number (or the horizontal Richardson number). The Simpson number is expressed as:

770
$$S_i = g\beta \frac{ds}{dy} \frac{h^2}{u_*^2}, \quad (87)$$

771 in which u_* is the bottom friction velocity, represented by $u_* = \sqrt{C_d}U_t$, where C_d is
772 the bottom friction coefficient and U_t is the tidal velocity amplitude.

773 When S_i lies in the range of 0.088 to 0.84, the water column stays periodically
 774 stratified, and the straining-induced circulation is an important component in the
 775 longitudinal estuarine circulation. When S_i is larger than 0.84, the water column is in
 776 a persistent stratified situation, and the straining-induced circulation becomes weaker.
 777 We calculated the S_i along the longitudinal section in different years and depict them
 778 in Fig. 1211.



779
 780 Fig. 1211. Distribution of the Simpson number in different years along the longitudinal section.
 781 The Y-axis represents the logarithmic of the S_i . The black dotted line represents the location
 782 of the null point.
 783

784 It indicates that along the longitudinal section, the S_i number was mostly above
 785 the criterion of 0.84, showing that the straining-induced circulation is not significant.
 786 The S_i number was the smallest in 2003 and the largest in 2010. It indicates that with
 787 the narrowing and deepening of the HE, the straining-induced circulation became
 788 weaker. This is consistent with Burchard et al. (2014) and Schulz et al. (2015). It
 789 indicates that with the human interventions, the straining-induced circulation became
 790 less important in the longitudinal estuarine circulation.

791 For the advection-induced longitudinal estuarine circulation, we noted that the
 792 longitudinal and vertical advection terms were smaller than the lateral advection. Based
 793 on Cheng and Valle-Levinson (2009), the lateral advection-induced longitudinal
 794 circulation is proportional to the ratio of $h/(wK_m)$, where w is the width, and K_m is
 795 the eddy viscosity. It shows that in a narrower and deeper estuary, the lateral advection
 796 has a larger effect in influencing the longitudinal estuarine circulation. Lerczak and

797 Geyer (2004) also showed that the effect of the lateral advection on longitudinal
798 circulation is stronger for narrower estuaries. Our results show that with the narrowing
799 and deepening of the estuary, not only the lateral advection but also the longitudinal
800 advection has great influences on the longitudinal estuarine circulation.

801

802 **4.4 The possible future development of the estuarine circulation and its** 803 **implications**

804

805 The pattern of lateral circulation during the dry season in the HE experienced a
806 dramatic change from 2003 to 2010 in the West Shoal at Sec. B2, from an under-
807 developed circulation structure to a complete clockwise vortex in 2010. This transition
808 was associated with the increase in lateral salinity gradient, the increase in longitudinal
809 bottom landward flow, and a decrease of friction by the increased water depth and
810 stratification.

811 The mechanisms for the lateral circulation during the wet season have been
812 revealed by Chen et al. (2020b), who showed that it was primarily driven by the
813 barotropic process, i.e., the water elevation gradient, and thus by the intensity of the
814 ebb jet. Different from the wet season when the river discharge was higher, the lateral
815 circulation in the dry season was more affected by the baroclinic effect. We speculate
816 that with the narrowing and deepening of the estuary, the lateral circulation even in the
817 wet season will be enhanced with the ebb jet in the deep channel strengthened.

818 In the HE, the channel underwent siltation, and sediment was carried from the
819 channels to side banks by the lateral circulation, making the estuary overall shallower
820 in 2003. In 2005, dredging of the channel increased the channel depth (Luo, 2010),
821 ~~resulting in a high deepening rate,~~ and increased the longitudinal estuarine circulation,
822 though the lateral circulation decreased slightly by the smaller rate of convergence. If
823 reclamation did not occur as frequently as it did in the last century, and the channel
824 dredging continued, the estuarine circulation of the estuary will in general keep
825 increasing with the increase in water depth, and ~~there exists~~ thus a positive feedback

826 **exists**. However, as revealed in Eq. (6) and Eq. (2) in Chant et al. (2018), with the
827 increase in salt intrusion, the longitudinal salinity gradient will decrease, showing
828 negative feedback. Moreover, Schulz et al. (2015) noted that estuarine circulation
829 exhibits a distinct maximum in medium-wide channels by comparing estuarine
830 circulation under different width-to-depth ratios. In our study, as shown in Table 4, the
831 width-to-depth ratio has been decreasing from 1977 to 2010, but the estuarine
832 circulation has been increasing. The difference would be caused by the fact that in our
833 study site, the tidal mixing is not strong enough to generate an effective tidal straining-
834 induced circulation.

835 The changes in the estuarine circulation have important implications for sediment
836 transport and morphological evolution in the HE. With the increase of longitudinal
837 estuarine circulation, the sediment trapping effect is expected to be enhanced, thus more
838 riverine sediment would be trapped inside the estuary. In the meantime, the change in
839 lateral circulation would decrease the sediment advection from the channel to the West
840 Shoal, which occurred in the wet season and was favorable for the siltation in the West
841 Shoal (Chen et al., 2020b).

842 In this study, the model used was only driven by river discharge and tides, without
843 considering the effects of winds, waves, and other upstream flows into the estuary.
844 Future work could incorporate the above factors to improve the model's accuracy.

845

846 **5. Conclusion**

847

848 This study investigated the morphological evolution of the HE from 1977 to 2010
849 using ArcGIS and remote sensing. It was noted that the West Channel of the HE
850 disappeared, causing the morphological pattern to change from “two channels and
851 three shoals” gradually to “one channel and two shoals” throughout the years. Due to
852 the reclamation and development of salt marshes along the estuarine banks, the estuary
853 has been experiencing continuous narrowing. Meanwhile, channel dredging has

854 deepened the estuary over the study period. The intensity of the longitudinal estuarine
855 circulation kept increasing as the estuary width continued to decrease. The trend of the
856 lateral circulation intensity altered when the estuary shallowed (from 1994 to 2003).

857 The changes in the longitudinal estuarine circulation were dominated by the
858 changes in the baroclinic pressure gradient force and advection. As the estuary was
859 narrowing and deepening, the pressure gradient force and advection term (especially
860 the horizontal advection term) increased, which increased the longitudinal circulation.
861 The change in lateral circulation intensity was mainly caused by the change of the
862 vertical shear of the longitudinal subtidal flow, the lateral salinity gradient, and the
863 vertical dissipation term. The changes in water depth were the dominant factor
864 affecting lateral circulation intensity. The increase of water depth enhanced the
865 longitudinal circulation and the lateral circulation of the upstream cross-section in
866 2010. The changes in the estuarine circulation have great implications for the sediment
867 transport in the HE, which would be explored in the next step.

868

869 **Data availability**

870 A total of 142G data of 66 images (Table 1) covering the PRD during cloudless days
871 in multiple years (from 1973 to 2018) were downloaded from <http://www.gscloud.cn/>.

872

873 **Author contributions**

874 RuiZhang: Writing - original draft, model runs and analyses. Bo Hong: Writing -
875 review. Lei Zhu: Writing - review. Wenping Gong: Writing - review & editing,
876 Conceptualization, Funding acquisition. Heng Zhang: Visualization, Funding
877 acquisition.

878

879 **Competing interests**

880 The authors declare that they have no conflict of interest.

881

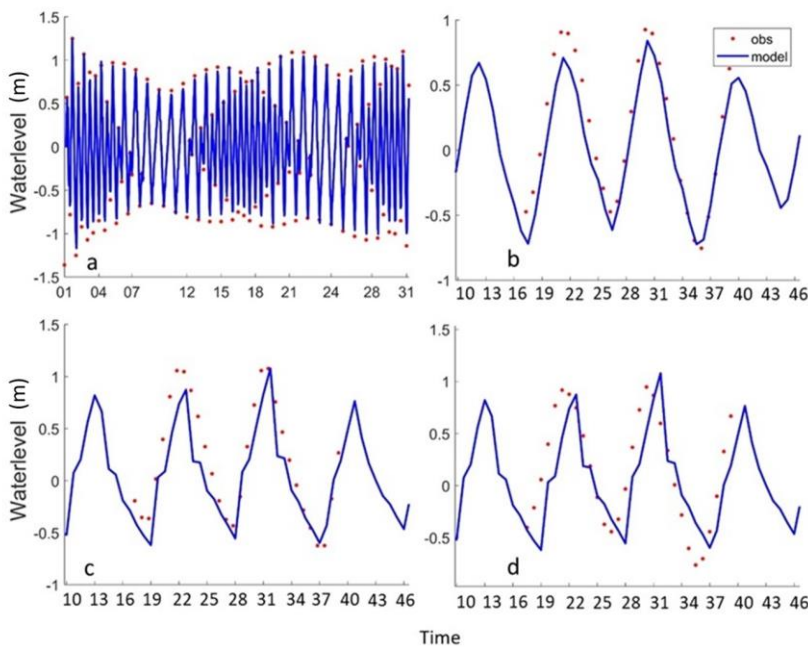
882 **Acknowledgments**

883 This research is funded by the National Natural Science Foundation of China [Grant
884 nos. 51761135021, 41506102, 41890851]. We would like to thank the National
885 Aeronautics and Space Administration (NASA) for providing the Landsat remote
886 sensing data. We are very grateful to graduate students in our team from Sun Yat-sen
887 for their help in fieldwork and sediment sample analysis in the indoor laboratory.

888

889

890 Appendix A



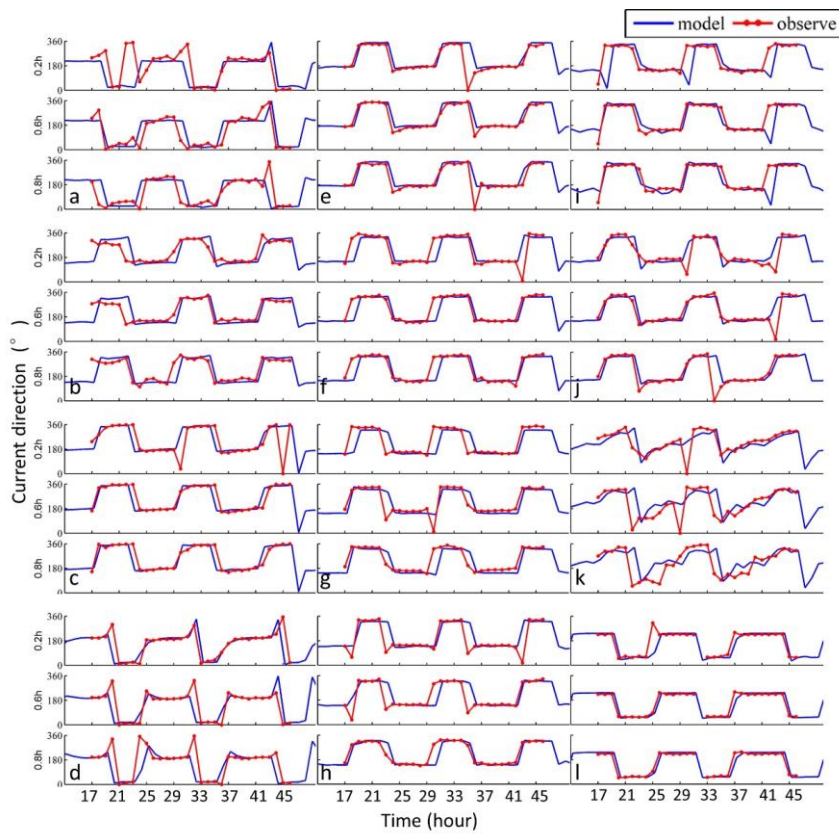
891

892 Fig. A. 1. Validation of water level of the MD2 model at 4 stations (S6 (a): SK=0.9969, DJ
893 (b): SK=0.9337, S1 (c): SK=0.8652, and GL (d): SK=0.8928) in March 2010. The red dots
894 and blue lines represent observation and simulated results, respectively. The station locations
895 are shown in Fig. 1b. Time in (a) is days from 2010/3/1, in (b-d) is hours from 2010/3/17-
896 00:00.

897

带格式的: 左, 1 级, 行距: 1.5 倍行距

带格式的: 1 级, 行距: 1.5 倍行距



带格式的: 左, 1 级, 行距: 1.5 倍行距

898

899 Fig. A. 2. Validation of current direction of the MD2 model at 12 stations (DJ (a), GL (b), HB

900 (e), S2(d), S3(e), S4(f), S5(g), S7(h), S6(i), S8(j), S9(k), and S1(l)) in March 2010. The red-

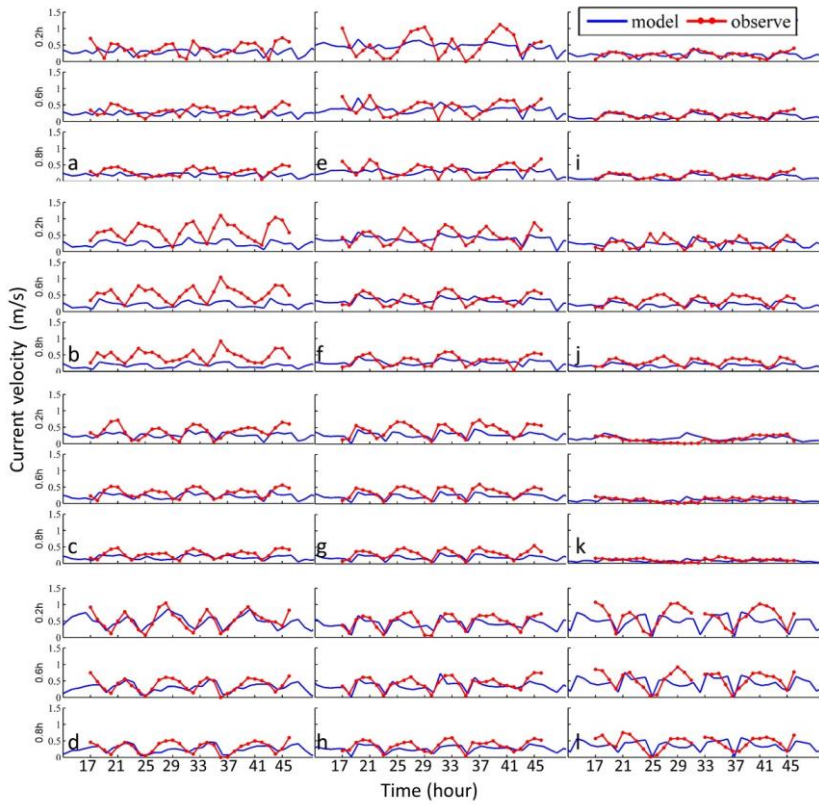
901 and blue lines represent observation and simulation results, respectively. The station locations-

902 are shown in Fig. 1b. Time is hours from 2010/3/17 00:00.

903

904

带格式的: 1 级, 行距: 1.5 倍行距



带格式的: 左, 1 级, 行距: 1.5 倍行距

带格式的: 1 级, 行距: 1.5 倍行距

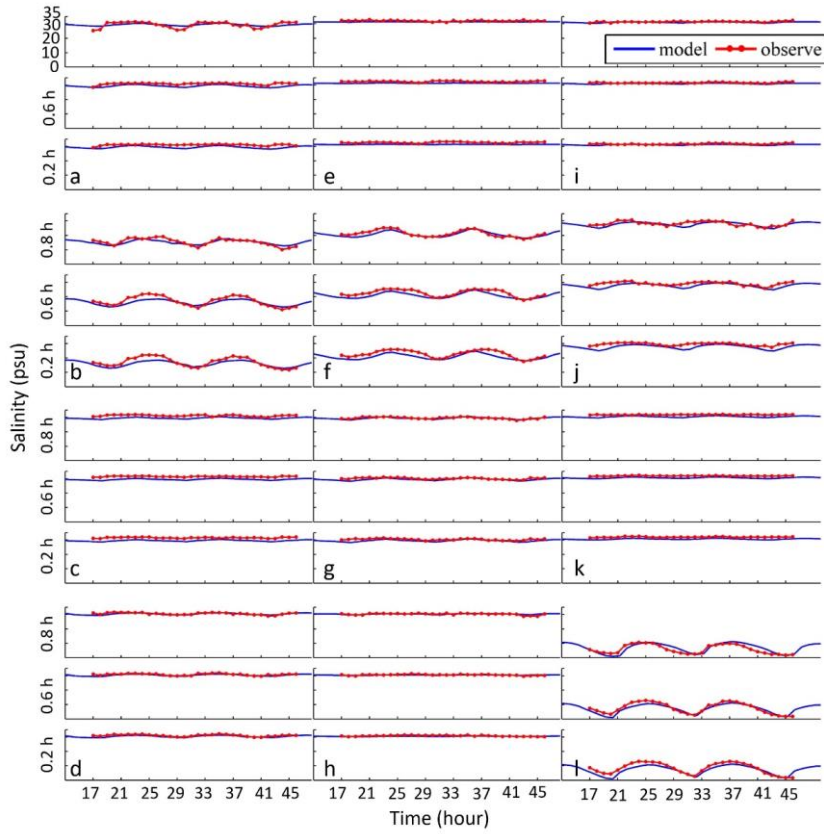
905

906 Fig. A. 3. Validation of current velocity of the MD2 model at 12 stations (DJ (a), GL (b), HB
 907 (e), S2(d), S3(e), S4(f), S5(g), S7(h), S6(i), S8(j), S9(k), and S1(l)) in March 2010. The red
 908 and blue lines represent observed and simulated results, respectively. The station locations are
 909 shown in Fig. 1b. Time is hours from 2010/3/17 00:00.

910

911

912



带格式的: 左, 1 级, 行距: 1.5 倍行距

913

914 Fig. A. 4. Validation of salinity of the MD2 model at 12 stations (DJ (a), GL (b), HB (c),
 915 S2(d), S3(e), S4(f), S5(g), S7(h), S6(i), S8(j), S9(k), and S1(l)) in March 2010. The red and
 916 blue lines represent observed and simulated results, respectively. The station locations are
 917 shown in Fig. 1b. Time is hours from 2010/3/17 00:00.

918

带格式的: 1 级, 行距: 1.5 倍行距

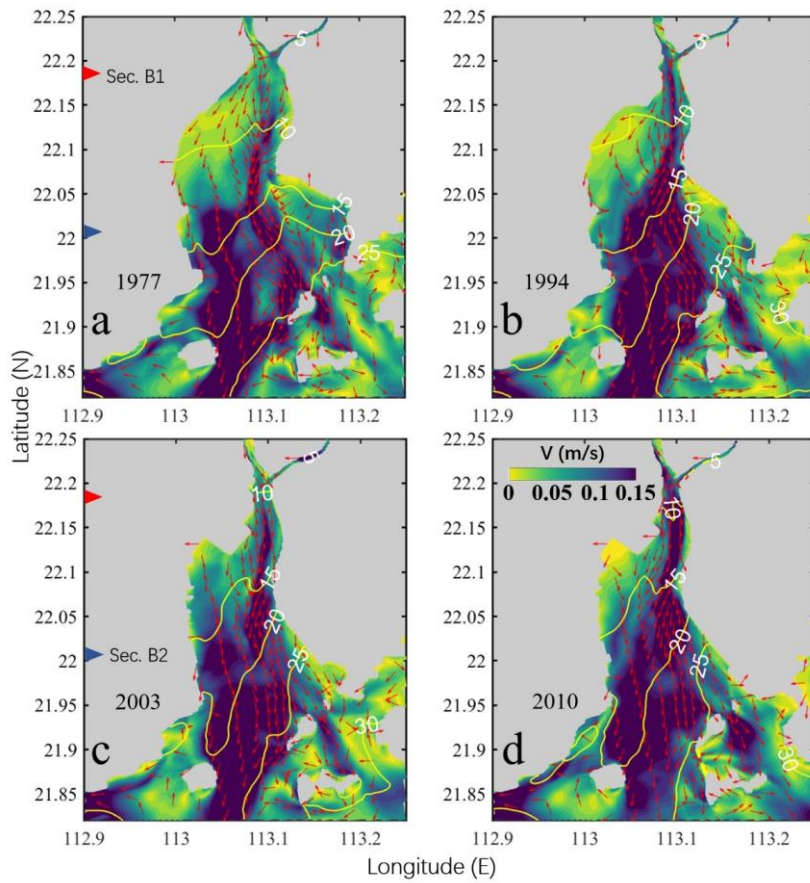
919

920

921

922

923



924

925 Fig. A. 51. Patterns of the horizontal circulation at the surface during neap tide in 1977(a1),
 926 1994(a2), 2003(a3), and 2004(a4). The magnitude of the current is represented by the color
 927 shading, while the current direction is shown by the arrows. The salinity is depicted by the
 928 contour lines. The red and blue triangles depict the positions of two cross-sections (Sec.B1 and
 929 Sec.B2).

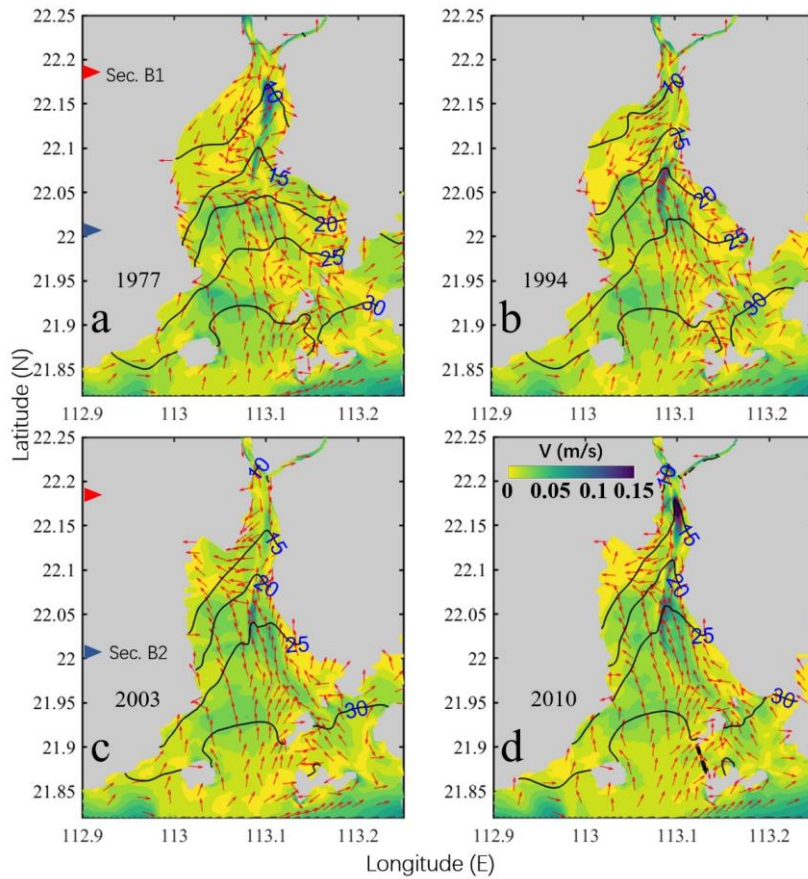
930

931

932

933

934



935
 936 Fig. A. 62. Patterns of the horizontal circulation at the bottom during neap tide in 1977(a1),
 937 1994(a2), 2003(a3), and 2004(a4). The magnitude of the current is represented by the color
 938 shading, while the current direction is shown by the arrows. The salinity is depicted by the
 939 contour lines. The red and blue triangles denote the positions of two cross-sections (Sec.B1 and
 940 Sec.B2).

941
 942
 943
 944
 945
 946
 947
 948

949 **References**

- 950
951 Ai, B., Zhang, R., Zhang, H., Ma, C. L. and Gu, F. G.: Dynamic process and artificial mechanism of
952 coastline change in the Pearl River Estuary, *Regional Studies in Marine Science*, 30, 100715, 2019.
- 953 Amin, M.: On perturbations of harmonic constants in the Thames Estuary, *Geophysical Journal of the*
954 *Royal Astronomical Society*, 73, 587-603, 1983.
- 955 Becherer, J., Stacey, M. T., Umlauf, L. and Burchard, H.: Lateral circulation generates flood tide
956 stratification and estuarine exchange flow in a curved tidal inlet, *J. Phys. Oceanogr.*, 45, 638-656,
957 2015.
- 958 Burchard, H., Hetland, R. D., Schulz, E. and Schuttelaars, H. M.: Drivers of Residual Estuarine
959 Circulation in Tidally Energetic Estuaries: Straight and Irrotational Channels with Parabolic Cross
960 Section, *J. Phys. Oceanogr.*, 41, 548-570, 2010.
- 961 Burchard, H., Schulz, E. and Schuttelaars, H. M.: Impact of estuarine convergence on residual circulation
962 in tidally energetic estuaries and inlets, *Geophys. Res. Lett.*, 41, 913-919, 2014.
- 963 Chant, R. J., Sommerfield, C. K. and Talke, S. A.: Impact of channel deepening on tidal and gravitational
964 circulation in a highly engineered estuarine basin, *Estuar. Coast.*, 41, 1587-1600, 2018.
- 965 Chen, L. H., Gong, W. P., Scully, M. E., Zhang, H., Cheng, W. C. and Li, W.: Axial wind effects on
966 stratification and longitudinal sediment transport in a convergent estuary during wet season, *Journal*
967 *of Geophysical Research: Oceans*, 125, e2019J-e15254J, 2020a.
- 968 Chen, L. H., Gong, W. P., Zhang, H., Zhu, L. and Cheng, W. C.: Lateral circulation and associated
969 sediment transport in a convergent estuary, *Journal of Geophysical Research: Oceans*, 125, e2019J-
970 e15926J, 2020b.
- 971 [Chen, S. N., Geyer, W. R., Ralston, D. K. and Lerczak, J. A.: Estuarine Exchange Flow Quantified with](#)
972 [Isohaline Coordinates: Contrasting Long and Short Estuaries, *J.phys.oceanogr.* 42, 748-763, 2012.](#)
- 973 Chen, S. N. and Sanford, L. P.: Axial Wind Effects on Stratification and Longitudinal Salt Transport in
974 an Idealized, Partially Mixed Estuary, *J. Phys. Oceanogr.*, 39, 1905-1920, 10.1175/2009JPO4016.1,
975 2009.
- 976 Cheng, P.: Decomposition of Residual Circulation in Estuaries, *Journal of Atmospheric & Oceanic*
977 *Technology*, 31, 698-713, 2013.
- 978 Cheng, P. and Valle-Levinson, A.: Influence of lateral advection on residual currents in microtidal
979 estuaries, *J. Phys. Oceanogr.*, 39, 3177-3190, 2009.
- 980 Cheng, P., Valle-Levinson, A. and De Swart, H. E.: Residual currents induced by asymmetric tidal
981 mixing in weakly stratified narrow estuaries, *J. Phys. Oceanogr.*, 40, 2135-2147, 2010.
- 982 Chernetsky, A. S., Schuttelaars, H. M. and Talke, S. A.: The Effect of Tidal Asymmetry and Temporal
983 Settling Lag on Sediment Trapping in Tidal Estuaries, *Ocean Dynam.*, 60, 1219-1241, 2010.
- 984 Dyer, K. R. 1977. Lateral circulation effects in estuaries. *National Academy of Sciences*, p. 22-29.
- 985 Eidam, E. F., Sutherland, D. A., Ralston, D. K., Dye, B., Conroy, T., Schmitt, J., Ruggiero, P. and Wood,
986 J.: Impacts of 150 Years of Shoreline and Bathymetric Change in the Coos Estuary, Oregon, USA,
987 *Estuar. Coast.*, 1-19, 2020.
- 988 Fischer, H. B.: Mixing and Dispersion in Estuaries, *Annu. Rev. Fluid Mech.*, 8, 107-133,
989 10.1146/annurev.fl.08.010176.000543, 1976.
- 990 Geyer, W. R.: Estuarine salinity structure and circulation, *Contemporary issues in estuarine physics*, 12,
991 26, 2010.

992 Geyer, W. R. and Maccready, P.: The Estuarine Circulation, *Annu. Rev. Fluid Mech.*, 46, 175-197, 2014.

993 [Geyer, W. R. and Nepf, H.: Tidal pumping of salt in a moderately stratified estuary, *Coastal and estuarine*](#)

994 [studies, 213-226, 1996.](#)

995 Gong, W. P., Jia, L. W., Shen, J. and Liu, J. T.: Sediment transport in response to changes in river

996 discharge and tidal mixing in a funnel-shaped micro-tidal estuary, *Cont. Shelf Res.*, 76, 89-107,

997 2014.

998 Gong, W. P., Liu, H., Ren, J. and Yu, H. B.: The study of tidal propagation in the Huangmaohai estuary

999 and its underlying mechanisms, *Acta Oceanol. Sin.*, 34, 41-54, 2012.

1000 Gong, W. P., Schuttelaars, H. and Zhang, H.: Tidal asymmetry in a funnel-shaped estuary with mixed

1001 semidiurnal tides, *Ocean Dynam.*, 66, 637-658, 2016.

1002 Huang, T. 2011. Study on abnormal changes of tidal range in the huangmaohai estuary. Guangdong

1003 Water Resources and Hydropower, Guangzhou, China.

1004 Jia, L. W., Luo, J. and Ren, J.: The analysis of the evolution of a sand bar and its formation in the

1005 Huangmao Bay in the Pearl River Delta, *Acta Oceanol. Sin.*, 34, 120-127, 2012.

1006 Kjerfve, B., Stevenson, L. H., Proehl, J. A., Chrzanowski, T. H. and Kitchens, W. M.: Estimation of

1007 material fluxes in an estuarine cross section: A critical analysis of spatial measurement density and

1008 errors I, *Limnol. Oceanogr.*, 26, 325-335, 1981.

1009 Lacy, J. R., Stacey, M. T., Burau, J. R. and Monismith, S. G.: Interaction of lateral baroclinic forcing and

1010 turbulence in an estuary, *Journal of Geophysical Research: Oceans*, 108, 1-34,

1011 <https://doi.org/10.1029/2002JC001392>, 2003.

1012 Lerczak, J. A. and Rockwell Geyer, W.: Modeling the Lateral Circulation in Straight, Stratified

1013 Estuaries*, *J. Phys. Oceanogr.*, 34, 1410-1428, 2004.

1014 Lesser, G. R., Roelvink, J. V., Van Kester, J. and Stelling, G. S.: Development and validation of a three-

1015 dimensional morphological model, *Coast. Eng.*, 51, 883-915, 2004.

1016 Li, C. Y. and O'Donnell, J.: Tidally driven residual circulation in shallow estuaries with lateral depth

1017 variation, *Journal of Geophysical Research Oceans*, 102, 27915-27929, 1997.

1018 Li, M., Cheng, P., Chant, R. J., Valle-Levinson, A. and Arnott, K.: Analysis of vortex dynamics of lateral

1019 circulation in a straight tidal estuary, *J. Phys. Oceanogr.*, 44, 2779-2795, 2014.

1020 Li, W., Shi, J. Z., Pu, X. and Hu, G. D.: Circulation within curved channel of the north passage in the

1021 changjiang river estuary: a vorticity approach, *Oceanologia et Limnologia Sinica*, 48, 682-694, 2017.

1022 Li, Y. B. 2019. Numerical simulation of the formation and evolution of the geomorphic characteristics

1023 of Huangmao Sea. Dalian University of Technology, Dalian, China.

1024 Luo, J. 2010. Cause Analysis of Morphological evolution of Huangmao sea Estuary in the Decade to

1025 Century-scale. Sun Yat-sen university, Guangzhou, China.

1026 Pritchard, D. W.: Salinity distribution and circulation in the Chesapeake Bay estuarine system.. 1, *Mar.*

1027 *Res*, 11, 106-123, 1952.

1028 Pritchard, D. W.: The dynamic structure of a coastal plain estuary, *J Marine Res*, 15, 33-42, 1956.

1029 Ralston, D. K. and Geyer, W. R.: Response to channel deepening of the salinity intrusion, estuarine

1030 circulation, and stratification in an urbanized estuary, *Journal of Geophysical Research: Oceans*,

1031 124, 4784-4802, 2019.

1032 Salles, P., Valle-Levinson, A., Sottolichio, A. and Senechal, N.: Wind - driven modifications to the

1033 residual circulation in an ebb - tidal delta: Arcachon Lagoon, Southwestern France, *Journal of*

1034 *Geophysical Research Oceans*, 120, 728-740, 2015.

1035 Schulz, E., Schuttelaars, H. M., Gr We, U. and Burchard, H.: Impact of the depth-to-width ratio of
1036 periodically stratified tidal channels on the estuarine circulation, *J. Phys. Oceanogr.*, 45, 411804097,
1037 2015.

1038 Scully, M. E., Geyer, W. R. and Lerczak, J. A.: The Influence of Lateral Advection on the Residual
1039 Estuarine Circulation: A Numerical Modeling Study of the Hudson River Estuary, *J. Phys.*
1040 *Oceanogr.*, 39, 107-124, 10.1175/2008JPO3952.1, 2009.

1041 Scully, M. E., Geyer, W. R. and Lerczak, J. A.: The Influence of Lateral Advection on the Residual
1042 Estuarine Circulation: A Numerical Modeling Study of the Hudson River Estuary, *J. Phys.*
1043 *Oceanogr.*, 39, 107-124, 10.1175/2008JPO3952.1, 2009.

1044 Scully, M., Friedrichs, C. and Brubaker, J.: Control of estuarine stratification and mixing by wind-
1045 induced straining of the estuarine density field, *Estuaries*, 28, 321-326, 10.1007/BF02693915, 2005.

1046 Simpson, J. H., Brown, J., Matthews, J. and Allen, G.: Tidal straining, density currents, and stirring in
1047 the control of estuarine stratification, *Estuaries*, 13, 125-132, 10.2307/1351581, 1990.

1048 Van Maren, D. S., van Kessel, T., Cronin, K. and Sittoni, L.: The impact of channel deepening and
1049 dredging on estuarine sediment concentration, *Cont. Shelf Res.*, 95, 1-14, 2015.

1050 [Wang, T., Geyer, W. R., Engel, P., Jiang, W. S. and Feng, S. Z.: Mechanisms of Tidal Oscillatory Salt](#)
1051 [Transport in a Partially Stratified Estuary, *J. Phys. Oceanogr.*, 45, 2773-2789, 2015.](#)

1052 Waterhouse, A., Tutak, B., Valle-Levinson, A. and Sheng, Y.: Influence of Two Tropical Storms on the
1053 Residual Flow in a Subtropical Tidal Inlet, *Estuar. Coast.*, 36, 1037-1053, 10.1007/s12237-013-
1054 9606-3, 2013.

1055 Willmott, C. J.: On the validation of models, *Phys. Geogr.*, 2, 184-194, 1981.

1056 Wilson, R. and Filadelfo, R. 1986. Subtidal Current Variability in the Lower Hudson Estuary. Springer -
1057 Verlag, Berlin, Germany. p. 132-142.

1058 Winterwerp, J. C.: Fine sediment transport by tidal asymmetry in the high-concentrated Ems River:
1059 indications for a regime shift in response to channel deepening, *Ocean Dynam.*, 61, 203-215, 2011.

1060 Zhang, R., Chen, L. H., Liu, S. S., Zhang, H. and Lin, G. Y.: Shoreline evolution in an embayed beach
1061 adjacent to tidal inlet: The impact of anthropogenic activities, *Geomorphology*, 346, 106856, 2019.

1062 Zhu, J., Weisberg, R. H., Zheng, L. Y. and Han, S. Z.: Influences of Channel Deepening and Widening
1063 on the Tidal and Nontidal Circulations of Tampa Bay, *Estuaries & Coasts*, 38, 132-150, 2015.

1064 Zhu, L. 2018. Alteration of estuarine circulation under the inference of morphological evolution. East
1065 China Normal University, Shanghai, China.

1066